© 2020. Published by The Company of Biologists Ltd | Journal of Cell Science (2020) 133, jcs237388. doi:10.1242/jcs.237388

RESEARCH ARTICLE

ORP3 phosphorylation regulates phosphatidylinositol 4-phosphate and Ca^{2+} dynamics at plasma membrane–ER contact sites

Gergő Gulyás[1,2], Mira Sohn[1], Yeun Ju Kim[1], Péter Várnai[2] and Tamas Balla[1,*]

ABSTRACT

Oxysterol-binding protein (OSBP)-related proteins (ORPs) mediate non-vesicular lipid transfer between intracellular membranes. Phosphoinositide (PI) gradients play important roles in the ability of OSBP and some ORPs to transfer cholesterol and phosphatidylserine between the endoplasmic reticulum (ER) and other organelle membranes. Here, we show that plasma membrane (PM) association of ORP3 (also known as OSBPL3), a poorly characterized ORP family member, is triggered by protein kinase C (PKC) activation, especially when combined with Ca^{2+} increases, and is determined by both PI(4,5)P_2 and PI4*P*. After activation, ORP3 efficiently extracts PI4*P* and to a lesser extent phosphatidic acid from the PM, and slightly increases PM cholesterol levels. Full activation of ORP3 resulted in decreased PM PI4*P* levels and inhibited Ca^{2+} entry via the store-operated Ca^{2+} entry pathway. The C-terminal region of ORP3 that follows the strictly defined lipid transfer domain was found to be critical for the proper localization and function of the protein.

KEY WORDS: ORP3, Phosphoinositides, Protein kinase C, STIM1, SOCE, TIRF, BRET

INTRODUCTION

Membrane contact sites (MCSs) between various organelles are emerging as key structural elements where important communication between organelles takes place (Gatta and Levine, 2017; Wu et al., 2018). They have been primarily featured in non-vesicular lipid transfer and Ca^{2+} signal propagation, but their importance is likely to reach beyond these two processes. An MCS is defined as the membrane apposition between membranes of two organelles with a distance no greater than 30 nm. While MCSs can be dynamic, they are stabilized by tethering proteins that also have functional roles. Several proteins have been identified that function in contact sites, including the extended synaptotagmins (ESyts) (Giordano et al., 2013; Manford et al., 2012) and many lipid transfer proteins (Wong et al., 2018). The ER Ca^{2+} sensor, STIM1 and the plasma membrane (PM) Orai1 channels also cluster in contact sites between the ER and PM to promote Ca^{2+} entry (Deng et al., 2009). Tethering proteins between the ER and mitochondria have also been shown to be important for Ca^{2+} transfer between these two organelles (Csordás et al., 2006; Szabadkai et al., 2006).

[1]Section on Molecular Signal Transduction, Eunice Kennedy Shriver National Institute of Child Health and Human Development, National Institutes of Health, Bethesda, MD, USA. [2]Department of Physiology, Faculty of Medicine, Semmelweis University, Budapest, Hungary.

*Author for correspondence (ballat@mail.nih.gov)

G.G., 0000-0002-5491-8699; T.B., 0000-0002-9077-3335

Received 1 August 2019; Accepted 29 January 2020

An important class of molecules that function at MCSs are the ORPs (oxysterol-binding protein-related proteins) (Kentala et al., 2016; Pietrangelo and Ridgway, 2018), which are mammalian orthologues of the yeast Osh proteins (Beh et al., 2012). The Osh/ORP proteins mediate the transport of specific lipids between cellular membranes, with their lipid cargo preference defined by their lipid transfer ORD (OSBP-related domain) domain (Pietrangelo and Ridgway, 2018). The best characterized members of this family are OSBP and its relatives, ORP5 (also known as OSBPL5), ORP8 (OSBPL8) and ORP2 (OSBPL2). Osh4 and OSBP were the first lipid transfer proteins in which the paradigm of phosphatidylinositol 4-phosphate (PI4*P*) gradient-driven cholesterol–PI4*P* counter-transport between the endoplasmic reticulum (ER) and the Golgi complex has been described (de Saint-Jean et al., 2011; Mesmin et al., 2013). ORP2 has been shown to mediate cholesterol transport between the ER and the PM controlled by PI(4,5)P_2 (Wang et al., 2018), whereas ORP5 and ORP8 proteins carry out the bidirectional transport of phosphatidylserine (PS) and PI4*P* between the ER and the PM (Chung et al., 2015). Less is known about the functions of other ORPs, particularly at ER–PM contact sites. Three additional ORPs, ORP3, ORP4 and ORP6 (OSBPL3, OSBPL4 and OSBPL6, respectively) have been reported to transfer lipids in membrane contact hotspots between the ER and PM (Mochizuki et al., 2018).

Generally, ORPs are anchored to the ER either with a C-terminal membrane spanning domain (in the case of ORP5 and ORP8) or via interaction of their FFAT (two phenylalanines in an acidic stretch) motifs with the ER-resident vesicle-associated membrane protein (VAMP) associated proteins (VAPs) (Loewen et al., 2003). The PM association of some of the ORPs is mediated by the interaction of their N-terminal PH domains with adjacent polybasic sequences with PM phosphoinositides, primarily with PI(4,5)P_2 and PI4*P* (Chung et al., 2015; Ghai et al., 2017; Sohn et al., 2018). Notably, however, not all yeast Osh proteins contain PH domains (Stefan et al., 2011).

While ORP3 has been shown to be associated with ER–PM contact sites (Mochizuki et al., 2018), recent studies also showed its presence in Rab7-positive endosomes, promoting their fusion with the nuclear envelope membrane (Santos et al., 2018). Binding of ORP3 to the PM requires protein kinase C activation, whereas its ER association is VAP protein dependent (Weber-Boyvat et al., 2015). Previous data showed that ORP3 has an important role in regulating cell adhesion due to its interaction with the small G-protein R-Ras (Weber-Boyvat et al., 2015). ORP3 overexpression also rescued the cellular phenotype associated with the P56S VAPB mutation linked to familial amyotrophic lateral sclerosis (Darbyson and Ngsee, 2016). In addition, ORP3 protein can form homo- or heterodimers with ORP6 while increasing PI4*P* turnover at the PM (Weber-Boyvat et al., 2015). Although these few selected cellular processes have been linked to ORP3, many details about its functions remain elusive.

Journal of Cell Science (2020) 133, jcs237388. doi:10.1242/jcs.237388

In the present study, we investigated the role of inositol lipids in the control of ORP3 function and conversely, the possible role of ORP3 in the organization of ER–PM contacts with respect to PI4*P* status and store-operated Ca^{2+} entry (SOCE). Our studies showed that association of ORP3 with the PM depends on PI4*P* and PI(4,5)P_2 levels at the PM, and on the ability of the protein to reduce PM PI4*P* levels and inhibit Ca^{2+} entry via SOCE. Our results also revealed an important role of the C-terminal portion of ORP3 in its ability to transport lipids and inhibit Ca^{2+} influx.

RESULTS

ORP3 requires PKC-dependent phosphorylation and VAP protein binding to form ER–PM contact sites

The lipid transport processes mediated by OSBP and several ORP proteins use the chemical gradient of PI4*P* for the counter-transport of selected lipid cargoes at MCSs (Antonny et al., 2018). This PI4*P* gradient partly relies on the ER-resident Sac1 phosphatase, which keeps PI4*P* levels low in the ER (Del Bel and Brill, 2018; Zewe et al., 2018) (Fig. 1A). To investigate the effect of ORP3 activation on PM phosphoinositide levels, we used HEK293 cells overexpressing ORP3. Since ORP3 requires ER attachment via the VAP proteins, we created an expression vector that contained two coding sequences expressed as two separate polypeptides at fixed stoichiometry: the ORP3 protein fused to the N-terminus of a fluorescent protein and the ER-resident protein VAPB separated by the viral T2A sequence (Fig. 1B). This approach allows simultaneous expression of two proteins with fixed stoichiometry (Tóth et al., 2012; Várnai et al., 2017). Transfection of HEK293-AT1 cells (a HEK293 cell line expressing the AT1 angiotensin II receptors; Hunyady et al., 2002) with this construct yielded the expected products, ORP3-Venus and VAP-B separately (Fig. 1C). To alter the lipid binding affinity of the ORD, we introduced three separate mutations (H631/632A, K829A and K837A) that were designed based on homology with the yeast OSH3, OSH4 and OSH6 proteins for which crystal structures were available (Tong et al., 2016). The H631/632A (HH/AA) mutation was shown to eliminate PI4*P* binding of the yeast OSH4 (de Saint-Jean et al., 2011; Maeda et al., 2013) and the mammalian ORP5 and ORP8 proteins (Chung et al., 2015; Ghai et al., 2017). We also generated a truncated form of ORP3 in which the C-terminus distal to the ORD domain was deleted (ORP3-ΔC-terminal-mCherry) or key hydrophobic residues within this domain were mutated ($ORP3^{FF/IL}$-mCherry and $ORP3^{WY/LL}$-mCherry) (Fig. 1B).

Confocal analysis of transiently transfected HEK293-AT1 cells was used to assess the ER association of the ORP3-Venus protein using mCherry-Sec61B as an ER marker (Fig. 1D) (for the single Venus channel of the same images, see Fig. S1). In agreement with published data (Weber-Boyvat et al., 2015), ORP3 localization to the ER was more pronounced in the presence of VAPB but no PM attachment was observed in unstimulated cells (Fig. S1A). Only after protein kinase C (PKC) activation by PMA (100 nM) treatment was the PM association visible (Fig. 1D and Fig. S1A). Notably, the ER–PM patches after PMA treatment were more pronounced with the $ORP3^{HH/AA}$ mutant (Fig. 1D and Fig. S1A). The PM association of these constructs was next analyzed by total internal reflection fluorescence (TIRF) microscopy. As shown in representative TIRF images in Fig. 2A, the number of PM patches developed after PMA treatment was again higher with $ORP3^{HH/AA}$ protein compared with the wild type. Although it appeared that puncta formation was more pronounced in several cells when VAPB was also expressed (Fig. 2A), this difference was not substantiated by analysis of a larger number of cells (Fig. 2B). Membrane association was quantified by measuring the average pixel intensity change following PMA treatment after background subtraction.

Phosphorylation of both endogenous ORP3 (Fig. 1C, lanes 1 and 2) and the Venus-tagged protein (Fig. 1C, lanes 4 and 5) was indicated by the slower mobility of the phosphorylated protein in SDS gels, although this difference was less marked with the larger, Venus-fused protein. This result suggested that PKC activation was necessary for PM association and that lipid cargo binding may exert an inhibitory effect on the PM binding process, as observed with other lipid transfer proteins (Kim et al., 2015).

PKC activation reduces PM PI4*P* levels in cells expressing ORP3

Given the ability of OSBP and some ORPs to transfer PtdIns4*P*, we wanted to know whether activation of ORP3 by PKC has any impact on PM phosphoinositide levels. For this, we monitored PM PI4*P*, PI(4,5)P_2 and PI(3,4,5)P_3 levels by bioluminescence resonance energy transfer (BRET) analysis in HEK293T cells expressing ORP3. Note that for most subsequent studies, we used HEK293-AT1 cells because of their utility to use receptor-mediated activation, but this early experiment was carried out in HEK293T cells, which expressed a higher level of the BRET constructs. The PMA-induced PI4*P* increase is more pronounced in these cells than in the HEK293-AT1 cells used in most of the current studies. The reason for this difference is not clear at present and was not pursued in this study, but it does not affect the conclusions regarding the effects of ORP3.

In control, mock-transfected cells, PMA treatment caused a slight elevation of PM PI4*P* and PI(3,4,5)P_3 levels, as observed earlier (Tóth et al., 2016). These changes were attributed to the activation of PI4K and Ras, respectively (Tóth et al., 2016). However, in cells expressing ORP3 (together with VAPB), PI4*P* showed a substantial decrease without any change in the other two phosphoinositides (Fig. 1E). The effects of ORP3 were similar but smaller in magnitude without VAPB co-expression, whereas VAPB alone had no effect (Fig. S1B). The PMA-induced PI4*P* decrease was greatly reduced in cells expressing $ORP3^{HH/AA}$, but it was not completely eliminated (Fig. 1E). Other mutants targeting PI4*P* binding (K829A or R837A) also reduced the effect of PMA, but neither has completely prevented the PI4*P* decrease (Fig. S1B,C). These results showed that PKC activation is required for triggering ORP3 function and that activated ORP3 can extract PI4*P* from the PM (Darbyson and Ngsee, 2016; Weber-Boyvat et al., 2015).

PM association of phosphorylated ORP3 depends on the PI4*P* and PI(4,5)P_2 content of the PM

Next, we investigated the mechanism by which the ORP3 protein binds to the PM. To determine if phosphoinositides are required for PM binding of ORP3, we acutely altered phosphoinositide levels in the PM of HEK293-AT1 cells using the recruitable phosphoinositide-modifying enzymes, pseudojanin (PJ)-Sac1 and PJ 5-phosphatase (PMA did not increase PI4*P* levels in these cells as opposed to HEK293T cells). These tools can be used to selectively reduce PM PI4*P* or PI(4,5)P_2 content or both (Gulyás et al., 2017; Hammond et al., 2012). To probe the potential role of the phosphoinositide 3-kinase (PI3K) products such as PI(3,4)P_2 and PI(3,4,5)P_3 in ORP3 PM targeting, a low concentration of wortmannin (Wm, 100 nM) was used to inhibit class I PI3Ks. These manipulations were combined with the expression of ORP3-Venus and its PM association was monitored by TIRF microscopy. We used the lipid-transport-deficient $ORP3^{HH/AA}$ mutant to mitigate its own effects on PM PI4*P* levels. In simultaneous experiments, the changes in PM phosphoinositides

Journal of Cell Science (2020) 133, jcs237388. doi:10.1242/jcs.237388

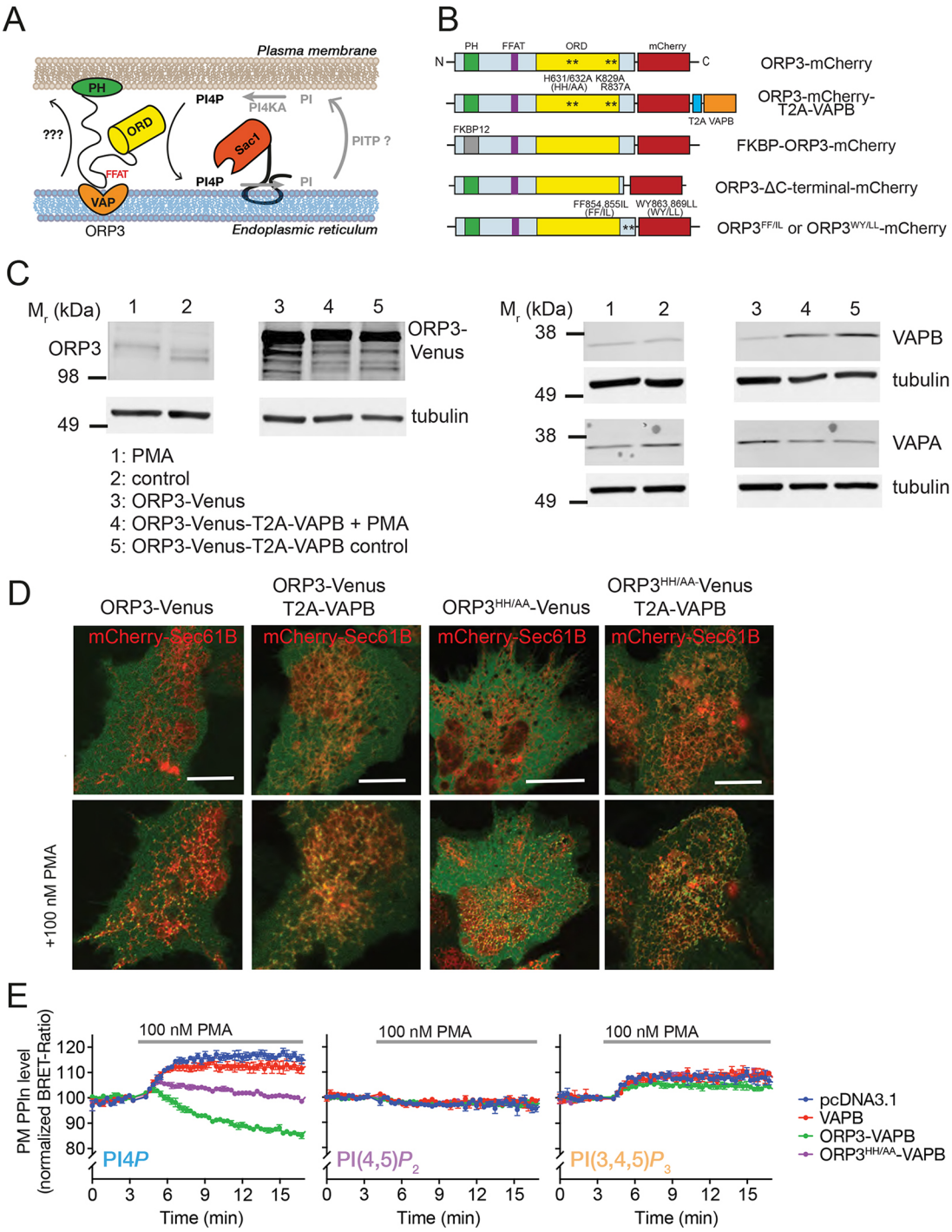

Fig. 1. PKC activation and VAP interaction are key determinants of ORP3 localization and function. (A) A simplified cartoon illustrating the operation of the ORP3 protein. ORP3 binding to the PM is mediated by the PH domain of the protein, whereas its ER binding is mediated by the FFAT motifs that interact with the ER-resident VAP proteins. The ER-resident PI4*P* phosphatase Sac1 and the PM-localized PI4KA enzyme maintain the PI4*P* gradient between the two membranes. (B) Schematic representation of the different ORP3 constructs used in this study. Although ORP3 has one FFAT-like and one genuine FFAT motif, only one is depicted here for simplicity. The approximate position of the mutations within the ORD domain are marked with asterisks. (C) Western blot analysis of ORP3 and VAP proteins in non-transfected HEK293-AT1 cells (lanes 1 and 2), or in cells expressing ORP3-mVenus (lane 3) or ORP3-mVenus-T2A-VAPB (lanes 4 and 5). 100 nM PMA was used for 10 min to activate PKC (lanes 1 and 4). Control treatment (lanes 2 and 5) was with DMSO. (D) Confocal images showing the intracellular localization of ORP3-Venus protein or ORP3$^{HH/AA}$ relative to the ER-marker mCherry-Sec61B transiently transfected HEK293-AT1 cells. In resting cells, both the wild-type and mutant ORP3-Venus show cytoplasmic localization. In the presence of VAPB, both constructs are partially ER-localized (these differences are better seen in the single Venus channel shown in Fig. S1A). After 100 nM PMA treatment (5 min), the proteins form patches on the PM, indicating PM and ER binding at contact sites. Scale bars: 10 µm. (E) Monitoring changes in PM phosphoinositide levels after ORP3 activation using BRET-based biosensors. HEK293T cells were transiently transfected with the respective BRET probes together with the indicated constructs. After a 5 min control period, cells were treated with 100 nM PMA to activate ORP3. BRET ratio values were normalized taking the resting ratio as 100% and the complete lack of energy transfer as 0% (for details, see Materials and Methods). Data are means±s.e.m. of three independent experiments, each performed in triplicate.

Journal of Cell Science (2020) 133, jcs237388. doi:10.1242/jcs.237388

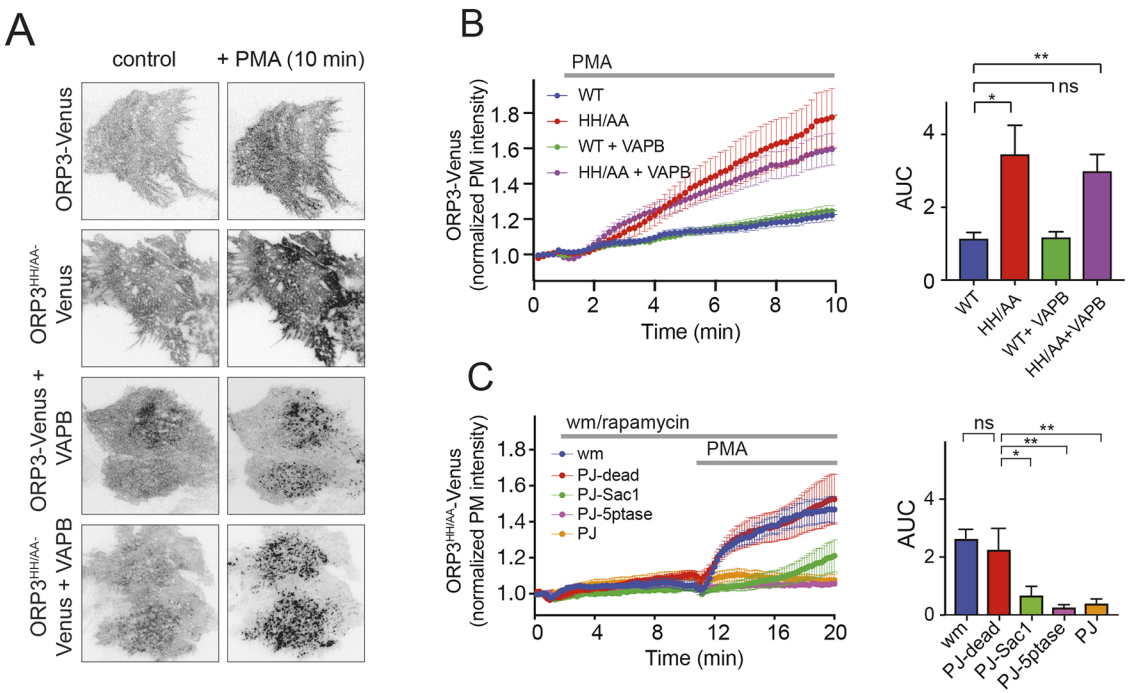

Fig. 2. Phosphoinositides determine the PM binding of ORP3 after PMA treatment. (A) Representative TIRF images show the footprint of HEK293-AT1 cells transfected with the indicated constructs. Selected images are shown from a time-lapse series showing the same cells before and 10 min after PMA addition. (B) Quantification of image sequences obtained in several TIRF experiments similar to that shown in A. For calculations of the normalized PM intensities, see the Materials and Methods. Bar diagrams show the area under the curve (AUC) values calculated from 7 (WT and ORP3$^{HH/AA}$), 14 (WT-VAPB) and 18 (ORP3$^{HH/AA}$-VAPB) independent dishes obtained in 2–8 experiments. Data are means±s.e.m. The PM binding of ORP3$^{HH/AA}$ was significantly higher than wild type regardless of the presence of VAPB. Welch ANOVA analysis was used to compare the groups with different sample sizes. The individual groups were compared with unpaired Welch *t*-test in multiple comparison (***P*<0.01; **P*<0.05; ns, not significant). (C) Monitoring the PM binding of the ORP3$^{HH/AA}$ protein (ORP3$^{HH/AA}$-mVenus-T2A-VAPB) in response to PMA stimulation after manipulation of the PM phosphoinositide pools. To selectively reduce PM PI4*P*, PI(4,5)P_2 or their combination, an inducible heterodimerization approach was employed utilizing the FKBP-fused pseudojanin (PJ) lipid phosphatase. PJ-Sac1 (4-phosphatase active, green curve) or PJ-5ptase (5-phosphatase active, purple curves) selectively deplete PM PI4*P* or PI(4,5)P_2, respectively. The dual activity PJ (both 4- and 5-phosphatase active) eliminates both of these phosphoinositide lipids. The enzymatically inactive protein (PJ-dead, red curve) was used as control. To reduce the PI3K products PI(3,4,5)P_3 and PI(3,4)P_2, 100 nM wortmannin (wm, blue curves) was added before the PMA stimulation. For the calculation of the normalized PM intensities, see the Materials and Methods. Bar diagrams show AUC values calculated for the period corresponding to PMA stimulation. Data are means±s.e.m. from 7 independent dishes in each group, obtained in 3–5 experiments. PM PI(3,4,5)P_3 and PI(3,4)P_2 depletion had no effect on the PM binding of the ORP3 protein, compared with the control cells (expressing PJ-dead). In contrast, the PM binding of ORP3$^{HH/AA}$ was significantly reduced after PM PI4*P* or PI(4,5)P_2 depletion (green and purple curves and bars, respectively), PI(4,5)P_2 depletion having a more robust effect. One-way ANOVA with Dunnett test was used to compare groups to the inactive enzyme (PJ-dead, red curves and bar) control (**P*<0.05; ***P*<0.01; ns, not significant).

were followed with previously described BRET sensors to verify the effects of the recruited lipid-modifying enzymes (Fig. S2).

Reducing PI4*P* levels in the PM with the recruitable PJ-Sac1 enzyme significantly decreased both the rate and the extent of ORP3$^{HH/AA}$ PM attachment compared with cells where the inactive PJ enzyme was expressed (Fig. 2C). Parallel BRET measurement showed that PI4*P* was selectively reduced in the PM after the recruitment of PJ-Sac1 (Fig. S2A). Even more profound inhibition of ORP3$^{HH/AA}$ PM binding was observed when the PJ 5-phosphatase or the fully active PJ (both 5- and 4-phosphatase active) was recruited to the PM prior to PMA stimulation (Fig. 2C). Again, the BRET results confirmed the expected phosphoinositide changes after PM recruitment of the respective enzymes (Fig. S2A). In contrast, Wm pre-treatment had no effect on PMA-induced ORP3$^{HH/AA}$ PM attachment (compared with the PJ-dead control), suggesting that PI(3,4)P_2 and PI(3,4,5)P_3 do not play an important role in ORP3 PM targeting (Fig. 2C). Confocal experiments showed that both of these phosphoinositide lipids were completely eliminated from the PM by Wm treatment (not shown). In the BRET experiment, the complete elimination of the lipids translates to a 60–80% decrease in BRET ratios (Fig. S2B) since the luciferase construct still had a small remaining effect on the membrane-bound Venus protein even when it is completely released from the membrane (also see Gulyás et al., 2017; Tóth et al., 2019, 2016). Overall, these data showed that PI(4,5)P_2 has the most important role in the PM binding of ORP3, while PI4*P* has a smaller, but still significant contribution. Our results did not show a significant role of the PI3K lipid products in ORP3 PM attachment.

Stimulation of Ca^{2+}-mobilizing receptors leads to strong ORP3 activation

So far, we have used PMA to stimulate PKC. Next, we wanted to examine whether activation of cells via Ca^{2+}-mobilizing receptors was able to affect ORP3 localization or function. This was of interest because receptor-mediated PLC activation stimulates PKC by a combination of cytoplasmic Ca^{2+} increase and diacylglycerol (DAG) production, whereas PMA only mimics DAG. Moreover, at full activation, PLC also decreases the levels of PM PI4*P* and PI(4,5)P_2 (Bojjireddy et al., 2014), both of which we just showed to be important for the PM binding of ORP3. For this reason, we used HEK293-AT1 cells and a range of concentrations of angiotensin II (AngII). Lower agonist concentrations elicit a Ca^{2+} signal and activate PKC without the massive transient depletion of PI4*P* and PI(4,5)P_2 that is observed when using high concentrations of the agonist.

Journal of Cell Science (2020) 133, jcs237388. doi:10.1242/jcs.237388

These studies showed that low AngII concentrations that did not appreciably decrease PI4*P* or PI(4,5)P_2 levels in mock-transfected cells, caused a decrease of PI4*P* in cells expressing ORP3 and VAPB (Fig. 3A, red curves). Higher agonist concentrations caused a transient decrease followed by a slow recovery in both PI4*P* and PI(4,5)P_2 levels in control cells (Fig. 3A, blue curves). In cells expressing ORP3 (with VAPB), the recovery of PI4*P* [but not of PI(4,5)P_2] was strongly inhibited (Fig. 3A, red versus blue curves). These data indicated that even at the slightly reduced steady-state PI(4,5)P_2 levels reached at later time points (>7 min) of 100 nM AngII stimulation, activated ORP3 can extract PI4*P* from the PM. The fact that we were unable to detect any changes in PI(4,5)P_2 levels due to ORP3 expression, suggested that ORP3 is unable to extract PI(4,5)P_2 from the PM. These data confirmed earlier observations that PI(4,5)P_2 levels can be maintained even at reduced steady state PI4*P* levels (Hammond et al., 2012; Bojjireddy et al., 2014; Nakatsu et al., 2012).

Since PKC activation by receptor stimulation results from the combined effects of DAG production and cytoplasmic Ca^{2+} elevation, we wanted to compare the effect of PMA treatment with that of the combination of PMA and thapsigargin (Tg) on PI4*P* changes in cells expressing ORP3 with VAPB. Tg activates the SOCE pathway by decreasing the ER luminal Ca^{2+} concentration via inhibition of the SERCA Ca^{2+} pump of the ER. As shown in Fig. 3B, Tg treatment, which had no effect of its own (red trace), clearly enhanced the effect of PMA in the activation of ORP3-mediated PI4*P* transport (green versus blue traces).

ORP3 PM binding is enhanced in the presence of elevated Ca^{2+}

After testing the effects of receptor stimulation on the ability of ORP3 to influence phosphoinositide levels, we wanted to examine the PM association of ORP3 when stimulating with PMA alone or via AngII receptors. We, again, used TIRF microscopy and ORP3$^{HH/AA}$, which has a largely reduced effect on PM PI4*P* levels (Fig. 3B). Also, we used low AngII concentrations (5 nM) that do not reduce PM PI4*P* or PI(4,5)P_2 levels (Fig. 3A). Stimulation with 5 nM AngII caused a rapid association of ORP3 with the PM, a response that was faster and larger than that observed with PMA (Fig. 4A) (compare Fig. 2B and Fig. 4A, blue traces). Again, the ORP3$^{HH/AA}$ protein showed significantly stronger and faster PM binding than the wild-type variant (Fig. 4A, red trace). The larger PM-translocation response of ORP3$^{HH/AA}$ to low level AngII stimulation compared with the response to PMA was consistent with a stronger PKC activation in case of receptor stimulation. Since PMA activation has no effect on cytoplasmic Ca^{2+}, whereas AngII stimulation evokes a Ca^{2+} increase, the role of Ca^{2+} was studied next.

To buffer the cytoplasmic [Ca^{2+}] elevation during AngII stimulation we pre-treated cells with BAPTA/AM (10 µM, 10 min) before stimulation. BAPTA loading caused a significantly slower and reduced PM-translocation response of ORP3$^{HH/AA}$ (Fig. 4A, green trace). In a reverse experiment, we examined whether increasing Ca^{2+} concentration by Tg on its own or combined with PMA would affect the PM-translocation response of ORP3$^{HH/AA}$. Treating cells with Tg alone resulted in a small and transient PM binding, which was

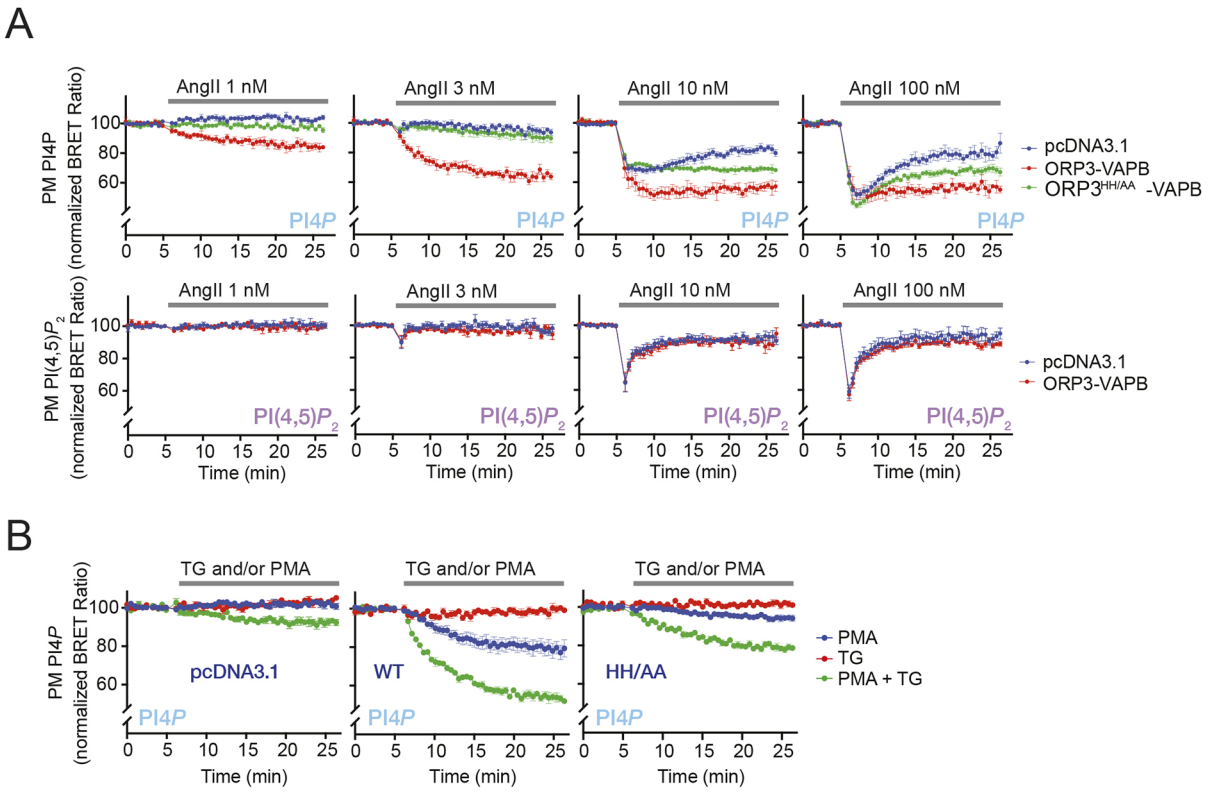

Fig. 3. The effect of ORP3 on PM phosphoinositide lipid changes during receptor stimulation or PMA and thapsigargin treatment. (A) Changes in PM PI4*P* and PI(4,5)P_2 levels after stimulation of angiotensin II (AngII) receptors that activate PLC. HEK293-AT1 cells were transiently transfected with the BRET biosensors monitoring PI4*P* (top panels) or PI(4,5)P_2 (bottom panels) together with the indicated constructs. Increasing concentrations of AngII were applied at the times indicated. Data are means±s.e.m. of three independent experiments each performed in triplicate. (B) Monitoring the effect of wild type and ORP3$^{HH/AA}$ on PM PI4*P* levels after treatment with either PMA (100 nM) or thapsigargin (Tg, 200 nM) or their combination. As a control, pcDNA3.1 was transfected instead of ORP3. Data are means±s.e.m. of three independent experiments, each performed in triplicate.

Journal of Cell Science (2020) 133, jcs237388. doi:10.1242/jcs.237388

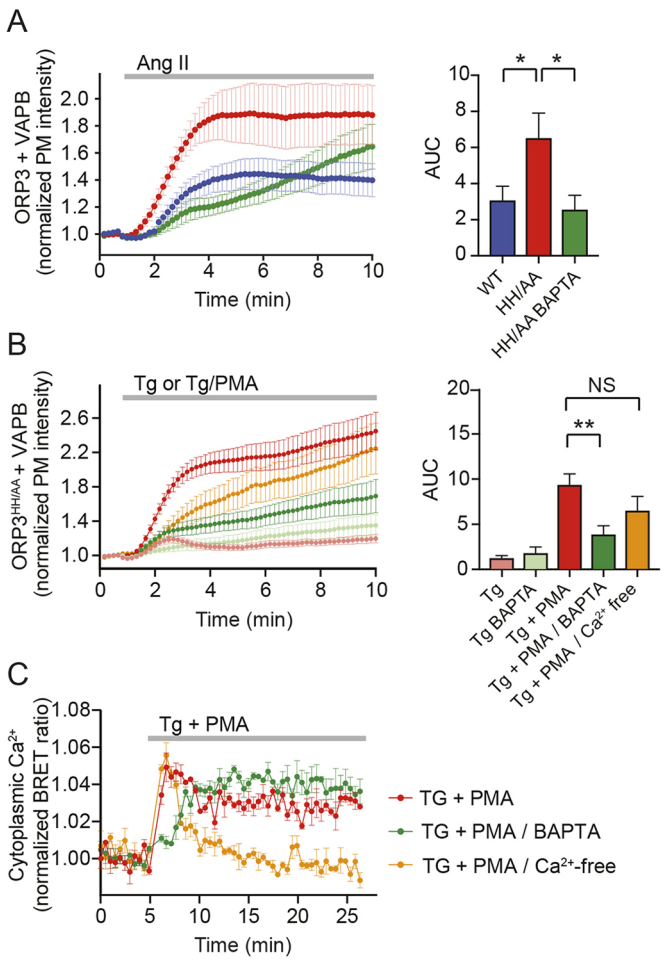

Fig. 4. Ca^{2+} influx contributes to the activation of ORP3. (A) Quantification of PM-binding of ORP3 or $ORP3^{HH/AA}$ with VAPB present in HEK293-AT1 cells stimulated with 5 nM AngII. Cells were transfected with the indicated plasmids and analyzed by TIRF microscopy. BAPTA-2AM loading (10 min, 10 µM) was carried out at room temperature. Data are means±s.e.m., recorded in [*n*=12 (WT), *n*=13 (HH/AA), *n*=7 (HH/AA-BAPTA)] independent dishes obtained in 3–7 experiments. Statistical analysis was carried out on the AUC values comparing different groups, as indicated, using unpaired *t*-test with Welch's correction (*P<0.05). (B) Similar experiments as shown in A except stimulation was with Tg (200 nM; tan and light green) or with a combination of Tg and PMA (red, dark green and orange). Cells were used with or without a 10 min pre-treatment with BAPTA-2AM (10 µM) as indicated. The nominally Ca^{2+}-free medium was supplemented with 100 µM EGTA. Data shown are means±s.e.m. of *n*=6 (Tg); *n*=7 (Tg BAPTA); *n*=13 (Tg+PMA); *n*=8 (Tg+PMA BAPTA) and *n*=7 (Tg+PMA/Ca^{2+} free) independent dishes obtained in 2–5 experiments. The AUCs were compared with unpaired Welch's *t*-test in multiple comparison. (**P<0.01; NS, not significant). (C) Cytoplasmic Ca^{2+} changes after stimulation of HEK293-AT1 cells with the combination of PMA (100 nM) and Tg (200 nM). Cells were transfected with the BRET-based intramolecular Ca^{2+}-sensor (Gulyas et al., 2015). Stimulation was carried out at the times indicated. BAPTA-2AM (10 µM) was used as pre-treatment for 10 min. The nominally Ca^{2+}-free medium was supplemented with 100 µM EGTA. Data are means±s.e.m. of three independent experiments, each performed in triplicate.

essentially eliminated in cells pre-treated with BAPTA/AM (Fig. 4B, tan and light green traces). However, the PM attachment became more pronounced after stimulation with PMA and Tg together, with the response comparable in size to that observed with AngII treatment (Fig. 4B, red trace). Pre-treatment of the cells with BAPTA effectively inhibited the PM translocation of $ORP3^{HH/AA}$ upon combined stimulation with PMA and Tg (Fig. 4B, green trace). Taken together, these data suggest an important role of the cytoplasmic [Ca^{2+}] increase in the activation process of ORP3, presumably because of the faster and more complete PKC activation compared with PMA treatment alone.

Store-operated Ca^{2+} entry (SOCE) is important for activation of ORP3

In addition to releasing Ca^{2+} from the ER, both agonist stimulation and Tg treatment activates store-operated Ca^{2+} entry (SOCE) (Liou et al., 2005; Zhang et al., 2005). Therefore, we investigated the role of SOCE and STIM1 in ORP3 PM binding, and contact site formation. First, we used Ca^{2+}-free medium (nominally Ca^{2+}-free medium, containing 0.1 mM EGTA) to eliminate Ca^{2+} influx during stimulation with Tg and PMA and studied the translocation response of the $ORP3^{HH/AA}$ mutant using TIRF analysis. As shown in Fig. 4B (orange trace), $ORP3^{HH/AA}$ translocation to the PM was reduced in Ca^{2+}-free medium, especially in the earlier phase. However, this difference was not statistically significant when calculated for the entire time period as the translocation response slowly approached the same level as seen in the presence of Ca^{2+}. Parallel cytoplasmic Ca^{2+} measurements using a BRET-based Ca^{2+} sensor (Gulyás et al., 2015) showed that the cytoplasmic Ca^{2+} increase was only transient in response to Tg and PMA in Ca^{2+}-free medium, reflecting Ca^{2+} release but no Ca^{2+} influx (Fig. 4C). In contrast, BAPTA loading buffered the early Ca^{2+} rise and slowed down the Ca^{2+} increase, which eventually reached similar plateau levels to those of Tg- and PMA-treated cells in normal medium (Fig. 4C, green trace). The strong effect of BAPTA on the association of $ORP3^{HH/AA}$ with the PM suggested that both the early rate of Ca^{2+} rise during combined Tg and PMA stimulation and increased Ca^{2+} influx had an important role in ORP3 activation.

Next, we examined whether the contact sites marked by STIM1 activation are the same or different from those occupied by activated ORP3. For this, we turned to COS-7 cells, which have a larger flat footprint and an elaborate network of tubular ER. Cells were transfected with ORP3-mCherry (together with VAPB) and a thymidine kinase-driven YFP-STIM1 construct and examined with confocal microscopy. Stimulation of cells either via the Gq-coupled endogenous P_{2Y} receptor by ATP, or Tg and PMA (Fig. 5A and B, respectively) caused clustering of both STIM1 and ORP3 and they showed good colocalization, suggesting that they were enriched in the same contact sites. The effect of STIM1 overexpression was also examined on $ORP3^{HH/AA}$ translocation to the PM in HEK293-AT1 cells (Fig. 5C). STIM1 overexpression had no effect when ORP3 translocation was examined after PMA stimulation (Fig. 5D, blue). Although STIM1 expression slightly enhanced the small response to Tg, this effect did not reach statistical significance (Fig. 5D, pink). Only when the cells were stimulated with Tg and PMA did STIM1 increase the translocation response of $ORP3^{HH/AA}$ (Fig. 5D, red). Again, BAPTA treatment largely reduced the $ORP3^{HH/AA}$ translocation response regardless of the presence of STIM1 (Fig. 5D, green).

Lastly, we wanted to determine the contribution of endogenous STIM1 to ORP3 PM attachment. For this, we knocked down STIM1 by siRNA and determined $ORP3^{HH/AA}$ PM translocation by TIRF microscopy. We also followed cytoplasmic Ca^{2+} changes using the BRET-based Ca^{2+} reporter during Tg and PMA stimulation. These experiments showed that STIM1 knockdown (Fig. 5F) significantly reduced the PM translocation of $ORP3^{HH/AA}$ following TG and PMA treatment (Fig. 5E) and also reduced the sustained phase of Ca^{2+} increase, consistent with its well-documented role in SOCE (Fig. 5G).

Journal of Cell Science (2020) 133, jcs237388. doi:10.1242/jcs.237388

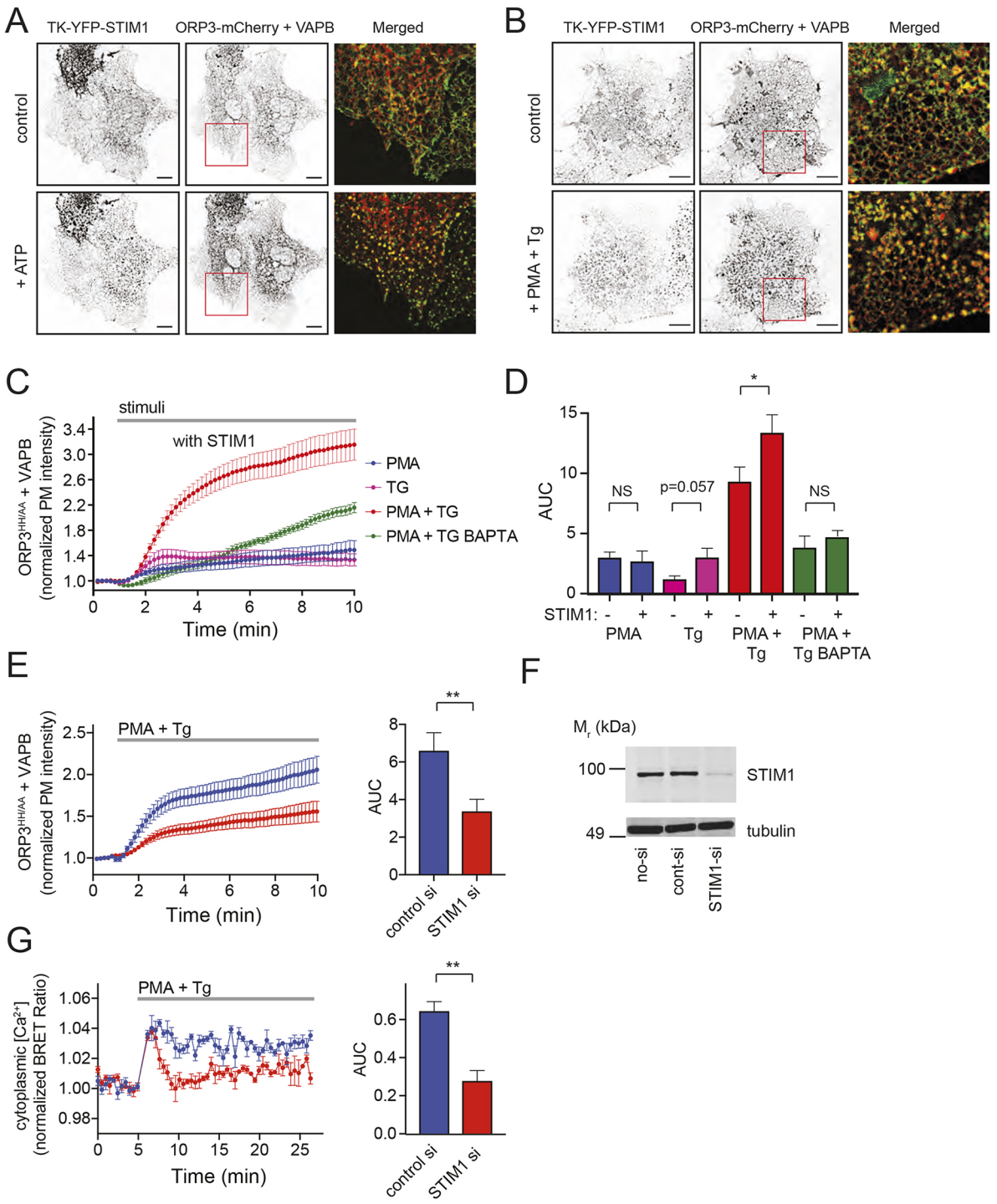

Fig. 5. The role of STIM1 on ORP3 PM binding. (A,B) Representative confocal images showing the colocalization between the wild-type ORP3 protein and STIM1 (TK-mRFP-STIM1) in COS-7 cells before and after stimulation with 50 µM ATP (A), or with a combination of 100 nM PMA+200 nM Tg (B). Red squares show the region enlarged in the merged images. Scale bars: 15 µm. (C) Membrane association of ORP3$^{HH/AA}$ in the presence of VAPB and STIM1 after stimulation with PMA (100 nM, blue), Tg (200 nM, pink) or their combination (red). When used, BAPTA-2AM (10 µM) pre-treatment was for 10 min (green). Data are means±s.e.m. of n=6 (PMA); n=7 (Tg); n=13 (PMA+Tg) and n=6 (PMA+Tg BAPTA) obtained in independent dishes acquired in 2–5 separate experiments. (D) Quantification of the TIRF experiments shown in C by calculating the AUC. The graph also includes data for the STIM1 minus groups obtained in experiments shown in Figs 2 and 4 for better comparison. Statistical differences were evaluated for each stimulus by comparing groups with or without STIM1 using unpaired t-test with Welch's correction (*P<0.05; NS, not significant). (E) Quantification of PM binding of ORP3$^{HH/AA}$ mutant (with VAPB) assessed in TIRF experiments using HEK293-AT1 cells stimulated with 100 nM PMA and 200 nM Tg. Cells were treated with either control siRNA (blue) or with siRNA against STIM1 (red). Data are means±s.e.m. of n=15 independent dishes for each group obtained in 4 experiments. The AUCs were compared using unpaired Welch's t-test (**P<0.01). (F) Western blot analysis of HEK293-AT1 lysates from cells treated with the indicated siRNA. The tubulin blot shown is from the same samples but run in a different gel. (G) Cytoplasmic Ca^{2+} changes after stimulation of HEK293-AT1 cells with the combination of PMA (100 nM) and thapsigargin (Tg, 200 nM). Cells were transfected with a BRET-based intramolecular Ca^{2+} sensor and stimulated as indicated. Data are means±s.e.m. of three independent experiments, each performed in triplicate. Statistical difference between the control and STIM1-silenced cells was calculated from AUCs using unpaired Welch's t-test (**P<0.01).

Journal of Cell Science (2020) 133, jcs237388. doi:10.1242/jcs.237388

ORP3 is able to extract PI4P but not PS, PI(4,5)P_2, DAG or cholesterol from the PM

Next, we explored whether lipids other than PI4*P* can be transported by the ORP3 ORD domain. For this, we used an ORP3 construct in which the PH domain was replaced with the FKBP module (Fig. 1B). This approach allows acute activation of ORP3 protein by acutely establishing its PM association using the PM-targeted FRB fragment of mTOR, as previously described for the ORP5 and ORP8 proteins (Sohn et al., 2018). To monitor changes in specific lipids in the PM after ORP3 activation, we used our previously described BRET-based PM lipid sensors for PI4*P*, PI(4,5)P_2, PI(3,4,5)P_3, PS and cholesterol (Sohn et al., 2018; Tóth et al., 2016).

As shown in Fig. 6A,B, rapamycin treatment caused a rapid decrease in PM PI4*P*, confirming the ability of the protein to extract PI4*P* from the PM. However, no decrease was observed when using the D4H-based cholesterol probe; in fact, a slight increase was observed in PM cholesterol levels after rapamycin treatment (Fig. 6A, B, red). In contrast, a slight decrease was observed with the PA-specific BRET probe (Fig. 5A,B, green). No changes were detected in PS, PI(4,5)P_2 or DAG levels using this approach (Fig. 6AB).

Activation of ORP3 inhibits SOCE

Given the presence of ORP3 and STIM1 in the same ER–PM contact sites, we investigated whether this colocalization has a functional consequence on Ca^{2+} signaling. For cytoplasmic [Ca^{2+}] measurements, we used the BRET-based Ca^{2+}-sensor in HEK293-AT1 cells. Cells were stimulated with increasing concentrations of AngII, which evoked bigger and bigger plateau Ca^{2+} elevations in control cells (Fig. 7A, blue curves). ORP3 expression together with VAPB reduced the Ca^{2+} plateau at higher AngII concentrations, and notably, the HH/AA mutant version was as effective as the wild-type protein (Fig. 7A, red and green curves). Other ORP3 mutants (K829A, R837A) that also impaired PI4*P* transport by these proteins (see Fig. S1B and C) had similar inhibitory effect (Fig. 7B). Importantly, no inhibition was detected when the VAPB protein was not expressed with the ORP3 proteins (Fig. S3B). We repeated these experiments using AngII together with Tg to prevent the refilling of the ER Ca^{2+} stores during AngII receptor desensitization. This manipulation allows better evaluation of any potential difference between the mutant and wild-type ORP3 proteins on Ca^{2+} signals. However, no difference was observed between the inhibitory effects of ORP3 or its mutants on these larger Ca^{2+} signals (Fig. 7C). Importantly, overexpression of the various ORP3 constructs did not prevent association of STIM1 with the PM (not shown).

Lastly, to determine if the inhibitory effect of ORP3 required its activation by PKC, we performed similar Ca^{2+} measurements using only Tg or Tg together with PMA in cells overexpressing ORP3 or $ORP3^{HH/AA}$ together with VAPB. These experiments showed that only when PMA was added together with Tg were the ORP3 proteins able to inhibit the Tg-induced Ca^{2+} elevations, and, again, the $ORP3^{HH/AA}$ protein was as effective as the wild type (Fig. 7D).

The C-terminal region adjacent to the ORD domain is critical for the localization and function of the ORP3 protein

The ORD domains of the Osh and ORP proteins show a large degree of conservation (Tong et al., 2016). The X-ray structures of yeast OSH3 and OSH4/Kes1 proteins show a long C-terminal segment that follows the conserved helix, the latter forming one side at the top of the lipid binding pocket (Fig. 8A). Interestingly, this C-terminal segment (labeled pink in Fig. 8A) is highly conserved among the various ORP3 orthologues (Fig. 8B). We investigated whether this region of the molecule has any importance for the function of the ORP3 protein.

First, we deleted the last 35 amino acid residues of ORP3 (ORP3ΔC) (Fig. 8B). This truncated ORP3 protein was also combined with the mutations that affected the lipid binding of the ORD domain. None of these truncated proteins was able to extract PtdIns4*P* from the PM following PMA and Tg treatment, even in the presence of VAPB (Fig. 8C). Moreover, none of these truncated ORP3 proteins were able to modulate Ca^{2+} signaling in Tg- and AngII-stimulated cells (Fig. 8D). Importantly, the C-terminally deleted ORP3 was still able to associate with the ER and increase its ER association after activation by Tg and PMA treatment (Fig. 8E). Yet, it showed no punctate structures after activation, suggesting that it no longer interacted with the PM (Fig. 8E). Although these features argued against a major folding problem, we generated single-residue mutations targeting conserved hydrophobic residues that were predicted to provide interaction with the core of the ORD

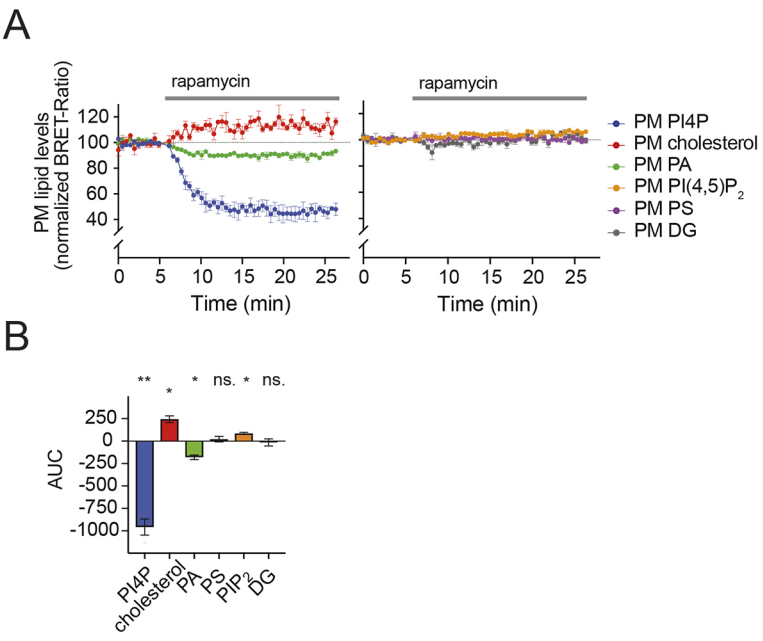

Fig. 6. Selected lipid changes in the PM after recruitment of the FKBP-tagged ORP3 protein. (A) The PH domain of ORP3 was replaced with FKBP12 allowing its rapid regulated recruitment to the PM. The FKBP12-ORP3-mCherry construct was co-transfected with the PM-anchored FRB (Lyn_{1-14}-FRB-mRFP), and the respective BRET sensors to monitor changes in the indicated lipids in the PM of HEK293-AT1 cells. Rapamycin (100 nM) was added after 5 min to recruit ORP3 to the membrane. Data are means±s.e.m. of three independent experiments, each performed in triplicate. (B) Bar diagrams showing the AUC calculations from the BRET experiments in A. Here, the areas were calculated relative to the baseline (0). For statistical analysis one-sample Student's *t*-test was used. Data are means±s.e.m. of three independent experiments, performed in triplicate (*P<0.05; **P<0.01; ns, non-significant).

Journal of Cell Science (2020) 133, jcs237388. doi:10.1242/jcs.237388

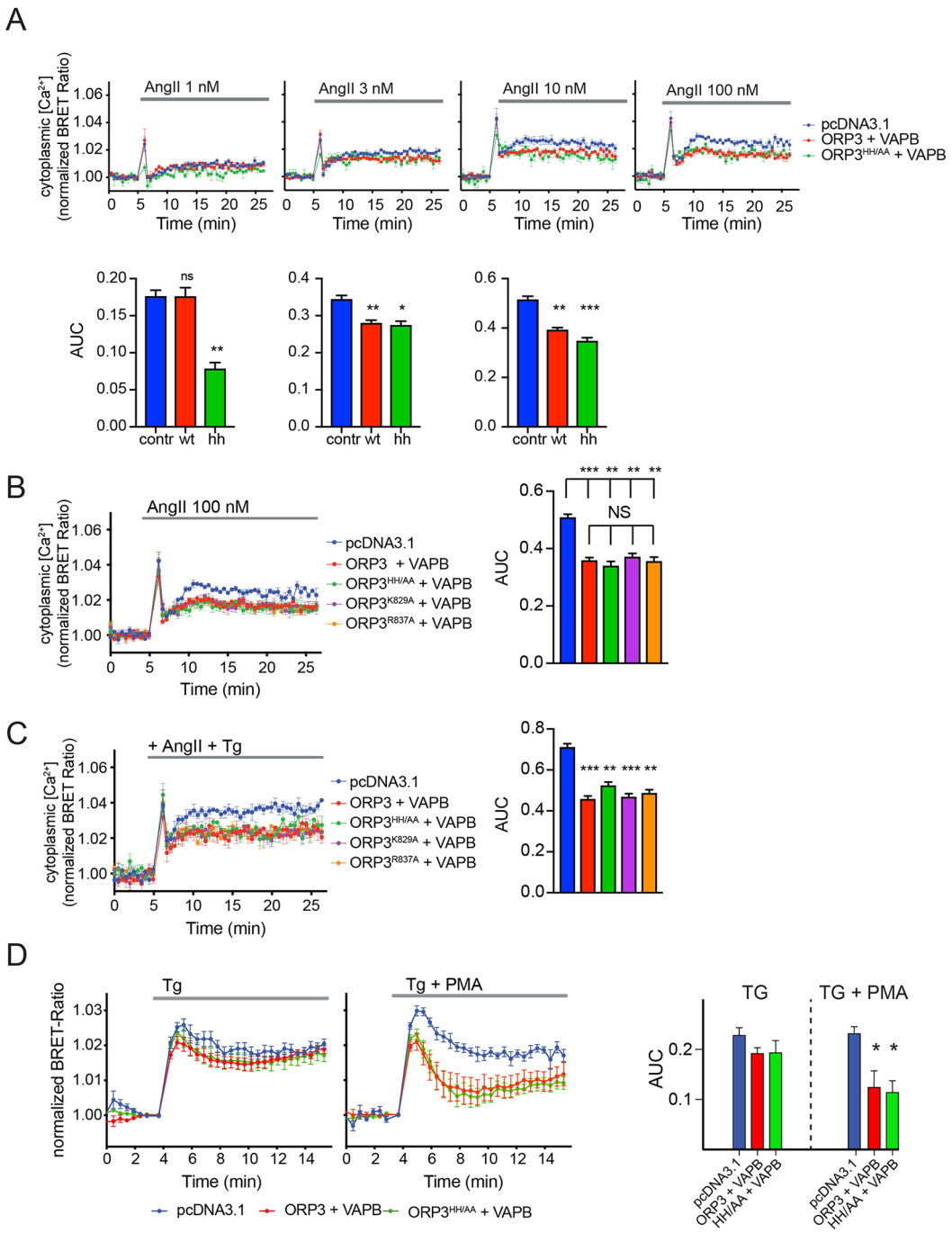

Fig. 7. ORP3 expression inhibits store-operated Ca^{2+}-influx. (A) Cytoplasmic Ca^{2+}-changes after stimulation of HEK293-AT1 cells with various concentrations of AngII. Cells were co-transfected with a BRET-based intramolecular Ca^{2+} sensor and the indicated ORP3 constructs with VAPB. AngII was added at the time indicated. Data are means±s.e.m. of three independent experiments, each performed in triplicate. Below each panel is the corresponding statistical analysis performed on the AUC values using Brown–Forsythe and Welch ANOVA, compared with the control (*P<0.05, **P<0.01, ***P<0.001). (B) Comparison of different ORP3 mutants on the cytoplasmic Ca^{2+} responses in HEK293-AT1 cells after stimulation with 100 nM AngII as described for A. Note that none of the mutants differed in their Ca^{2+} responses from that of the wild-type ORP3. The 100 nM AngII control curve (blue) shown in panel A is plotted here for comparison. Data are means±s.e.m. of three independent experiments, each performed in triplicate. The statistical analysis performed as described for A is shown on the right. (C) Similar experiments as shown in B, except stimulation was with AngII (100 nM)+Tg (200 nM). Data are means±s.e.m. of three independent experiments, each performed in triplicate. The statistical analysis is shown on the right. (D) Cytoplasmic [Ca^{2+}] changes in HEK293T cells, expressing the Ca^{2+}-sensitive BRET probe and the indicated ORP3 constructs. Cells were treated either with Tg (200 nM) alone, or in combination with PMA (100 nM) as indicated. Note that only after PKC activation does ORP3 exert an inhibitory effect. Data are means±s.e.m. of four independent experiments, each performed in triplicate. The statistical analysis performed as in A, is shown on the right (*P<0.05).

domain (labeled cyan in Fig. 8A). These mutants [F854I, F855L (FF/IL) and W863L, Y869L (WY/LL)] completely reproduced the behavior of the C-terminally deleted form.

Taken together, these data suggest that this C-terminal region of ORP3 (and perhaps other ORPs) plays an important role most likely by stabilizing the position of the long, conserved helix and

Journal of Cell Science (2020) 133, jcs237388. doi:10.1242/jcs.237388

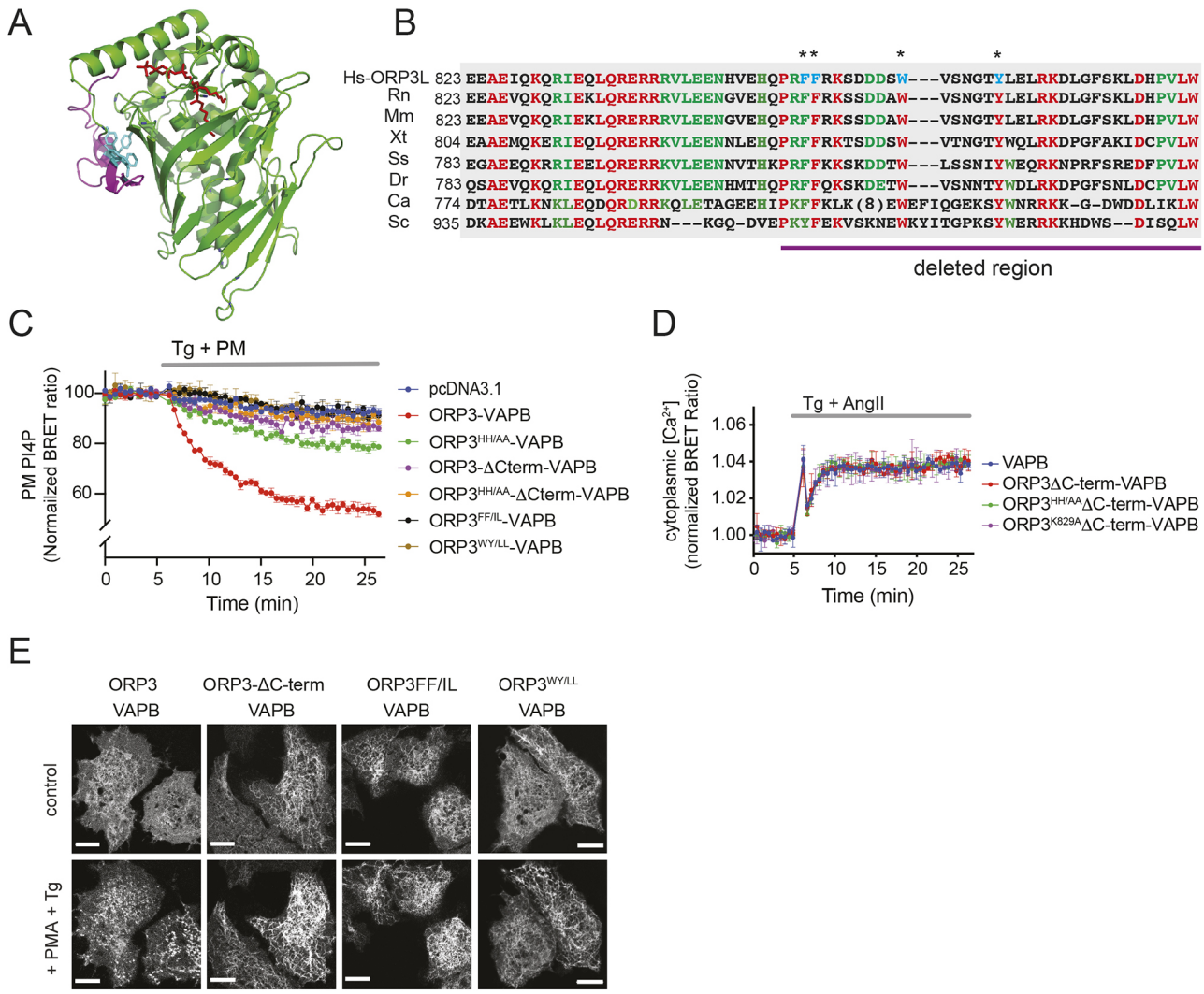

Fig. 8. Modification of the C-terminus of ORP3 eliminates lipid transport, PM binding and inhibition of Ca^{2+} signals. (A) 3D structure of the ORP3 ortholog OSH3 protein in complex with PI4P (4INQ) (Tong et al., 2013). The extreme C-terminal segment distal to the ORD domain and the conserved hydrophobic residues facing the ORD domain are highlighted in magenta and cyan, respectively. Pymol was used to generate this image. (B) Multiple alignment of the C-terminal ends of ORP3 orthologues. Conserved residues are marked red, partially conserved residues and conserved substitutions are marked green. The mutated conserved hydrophobic residues are marked with asterisks, and also highlighted in cyan within the human sequence. Hs, *Homo sapiens*; Rn, *Rattus norvegicus*; Mm, *Mus musculus*; Xt, *Xenopus tropicalis*; Ss, *Salmo salar*; Dr, *Danio rerio*; Ca, *Candida albicans*; Sc, *Saccharomyces cerevisiae*. (C) Effect of C-terminal truncation and mutagenesis of selected hydrophobic residues on the ability of ORP3 to affect PM PI4*P* levels in HEK293-AT1 cells. Cells were transiently transfected with the PI4*P*-specific BRET probe, and the indicated ORP3 mutants with VAPB. Activation of ORP3 proteins was induced by 100 nM PMA added after 5 min. Data are means±s.e.m. of three independent experiments, each performed in triplicate. (D) Cytoplasmic Ca^{2+} levels in HEK293-AT1 cells expressing a BRET-based Ca^{2+} sensor and the indicated ORP3 mutants with VAPB. Stimulation was with a combination of AngII (100 nM) and Tg (200 nM). Data are means±s.e.m. of three independent experiments, each performed in triplicate. (E) Confocal images of HEK293-AT1 cells showing the intracellular localization of the Venus-tagged versions of the wild-type ORP3-VAPB protein and its C-terminal region mutants as indicated. After 100 nM PMA and 200 nM Tg treatment (5 min), the wild-type protein forms patches on the PM, indicating PM and ER binding at contact sites. The patch formation is missing in the case of the mutants; however, increased ER binding is indicated by the drop in the background cytoplasmic fluorescence. Scale bars: 10 µm.

thereby allowing retention of the lipid cargo within the lipid binding pocket.

DISCUSSION

The present study was designed to investigate the properties and possible regulatory role of the ORP3 protein in PM–ER contact sites. The unique feature of ORP3 compared with OSBP and some other ORPs is that it requires PKC activation to induce a molecular rearrangement in order to display its membrane interaction and lipid transport ability (Weber-Boyvat et al., 2015). Little is known about the functions and regulation of ORP3, although the protein has been linked to focal adhesions, by regulating β1-integrin and R-Ras activity (Lehto et al., 2008; Weber-Boyvat et al., 2015), and its depletion causes aneuploidy and possibly contributes to cancer progression (Njeru et al., 2019).

In this paper, we found that the primary determinants of ORP3 PM binding are PI4*P* and PI(4,5)P_2 in the PM, but PM binding only occurs after PKC activation. A previous study using the isolated PH domain of ORP3 found its binding preference to PI(3,4,5)P_3 and PI(3,4)P_2, but our experiments using intact cells could not confirm the role of these lipids in bulk PM binding of ORP3. We cannot rule out the possibility that the 3-phosphorylated lipids play a role in localized enrichment of the protein in specific PM compartments, such as in focal adhesions, or in other locations within the cell. For

Journal of Cell Science (2020) 133, jcs237388. doi:10.1242/jcs.237388

example, recent studies have shown an important role of ORP3 in entry of late endosomes to the nucleoplasmic reticulum (Santos et al., 2018), a defect that may be related to the aneuploidy observed in ORP3-depleted cancer cells (Njeru et al., 2019). Although PI(4,5)P_2 has been shown to be present in late endosomes (Baba et al., 2019), it is possible that other phosphoinositides, such as PI(3,4)P_2 control ORP3 function in those compartments.

It has also been shown earlier that PKC-mediated phosphorylation regulates the attachment of ORP3 to VAPA (Weber-Boyvat et al., 2015). While we did not focus on this aspect of ORP3 regulation, we confirmed that PMA treatment caused a mobility shift in the migration of ORP3 in SDS gel electrophoresis consistent with its phosphorylation, and our studies also showed that binding of ORP3 to the PM phosphoinositide was also regulated by PKC activation. Based on these data, it is most likely that phosphorylation induces a major conformational change in ORP3 and opens the protein from a closed conformation that masks interaction of both the N-terminal PH domain and the FFAT motifs with their respective binding partners.

Recent studies have shown that phosphoinositides, particularly PI(4,5)P_2 and PI(3,4)P_2, control the lipid cargo loading of the ORD domains of ORP1 and ORP2 (Dong et al., 2019; Wang et al., 2018). In fact, the presence of a PH domain is not necessary for the functions of some of the yeast Osh proteins, such as Osh4/Kes1 (Maeda et al., 2013). The role of the PH domain (and adjacent sequences) in metazoan and some yeast OSBP homologues is to facilitate membrane interaction and localization of these proteins to membrane contact sites. Consistent with these ideas, replacing the PH domains with FKBP preserves the cargo transfer ability of the ORP3 protein and makes it inducible after establishing PM binding with rapamycin-mediated heterodimerization. Using this approach, we showed that the main phospholipid cargo of ORP3 protein is PI4*P*. Of the other lipids examined, we found a slight decrease in PM PA after ORP3 activation and a slight elevation in PM cholesterol. This latter finding might indicate a PI4*P*-coupled counter-transport of cholesterol to the PM by ORP3, but most likely, the main lipid cargo of this protein still awaits identification. The observed PA changes could reflect a direct ORP3-mediated PA transport or could be, again, an indirect consequence of PI4*P* transfer.

The most important and robust lipid change observed after ORP3 activation was the substantial depletion of PI4*P* in the PM. This suggested that ORP3 belongs to the increasing number of ORPs that use PI4*P* as a lipid cargo. Interestingly, mutations (HH/AA, K829A and R837A) within the ORD domain that have been shown to grossly decrease, if not eliminate, PI4*P* binding (Chung et al., 2015; de Saint-Jean et al., 2011; Maeda et al., 2013), have greatly reduced but did not fully eliminate the PI4*P*-depleting effect of ORP3. This may indicate a residual PI4*P* binding of the ORD domains, but also raised the possibility that ORP3 protein could stabilize ER–PM contacts and facilitate a possible action of Sac1 on PM PI4*P* in trans as speculated for Osh3 (Stefan et al., 2011). While the trans activity of Sac1 is not likely to be a major factor at the PM under physiological conditions (Zewe et al., 2018), it may become appreciable when promoting ER–PM contacts with expressed proteins. Curiously, a modification that completely eliminated all the activities of ORP3 was a truncation at its C-terminus or mutations that are expected to weaken its interaction with the ORD proper. This region is highly conserved among ORP3 orthologues, including Osh3 (Fig. 7B). Based on the structure of Osh3, this part of the molecule is not directly involved in cargo binding and contains solvent exposed positively charged and hydrophobic amino acids that may confer a binding surface for either an intramolecular interaction or interaction with another protein partner. The intramolecular interaction that is mediated by the hydrophobic residues mutated in this study could determine and stabilize the position of the long helix that borders the cargo binding hydrophobic pocket (Fig. 7A). More studies will be needed to characterize the role of this segment of the molecule in its activation and lipid transfer activities.

An important finding of our study was the synergistic effect of Ca^{2+} and PMA in evoking a maximal activation of ORP3. This explains the more robust activation of ORP3 during stimulation of receptors that activate PLC. Even at concentrations of agonists that reduce steady-state PI(4,5)P_2 and PI4*P* levels, there was enough phosphoinositide in the PM to support ORP3 activation. Our studies comparing the effects of BAPTA loading, removal of external Ca^{2+} or knockdown of STIM1 on ORP3 membrane association suggested that both the rate of Ca^{2+} rise and the sustained Ca^{2+} influx through the SOC channels were important for the full activation and PM association of the protein. The fact that STIM1 knockdown had a larger effect on ORP3 PM association than removal of external Ca^{2+}, raised the possibility that STIM1-mediated PM–ER contacts, which occur after ER store depletion even without external Ca^{2+}, could help ORP3 accumulation in this compartment. Conversely, overexpressed STIM1 increased ORP3 PM association simply by promoting and enlarging those ER–PM contact areas.

Lastly, our data revealed a potent inhibitory effect of ORP3 on Ca^{2+} signaling via SOCE. A previous study using targeted aquorin as a Ca^{2+} sensor showed that ORP5 and ORP8 overexpression increased Ca^{2+} concentration in caveolar microdomains and in mitochondria but was without effect on cytoplasmic Ca^{2+} changes evoked by histamine stimulation (Pulli et al., 2018). Since ORP3 activation leads to PM PI4*P* depletion, an obvious explanation for this inhibitory effect was a change in PM PI4*P*. Previous data suggested that SOCE is sensitive to PM phosphoinositide levels, as the C-terminal polybasic domain of STIM1 binds to acidic phospholipids such as PI(4,5)P_2 (Liou et al., 2007). Notably, the role of the different phosphoinositide levels has been a matter of debate, because PI4*P*, rather than PI(4,5)P_2, was suggested by three studies as the more important lipid in this context (Broad et al., 2001; Korzeniowski et al., 2009; Nakatsu et al., 2012). However, the inhibitory effect of ORP3 was also observed with mutants that were unable to achieve the same PI4*P* depletion as the wild type, and only the C-terminally-deleted or mutated ORP3 mutants were without effect. This raised the possibility that the ORP3 effect on SOCE may not be solely mediated by changes in phosphoinositides. The close physical proximity of the ORP3 proteins to the components of the STIM1–Orai1 machinery raise the question of whether there is a direct interaction between ORP3 and one or more of these proteins. Alternatively, a secondary change in the lipid composition of the PM caused by the increased presence of ORP3 could be responsible for this effect. While the exact mechanism of how this inhibition takes place is a matter of further investigation in our laboratory, it is intriguing that the sensitivity of ORP3 to SOCE-mediated Ca^{2+} increases is associated with an inhibitory effect of ORP3 on the very same process.

In summary, our studies have revealed several features of ORP3 activation; its binding to PM PI(4,5)P_2 and PI4*P*, the synergistic role of combined Ca^{2+} and DAG signals in ORP3 activation and the intimate reciprocal relationship between ORP3 and SOCE. The importance of the C-terminal domain of ORP3 activation and lipid transport suggests an evolutionarily conserved feature that will require further studies to be fully understood.

Journal of Cell Science (2020) 133, jcs237388. doi:10.1242/jcs.237388

MATERIALS AND METHODS

Materials

All molecular biology reagents were from New England Biolabs unless specified otherwise. For the polymerase chain reaction, the Pfu Turbo Hotstart polymerase was used (Agilent Technologies). Lipofectamine 2000 was purchased from Thermo Fisher Scientific. White flat bottom 96-well plates obtained from Corning were used in the BRET experiments. Eight-well µ-Slides for confocal experiments were ordered from IBIDI (Cat. No. 80826), while glass bottom single dishes for TIRF experiments were from CellVis (Mountain View, CA, USA). Coelenterazine h was purchased from Regis Technologies (Morton Grove, IL, USA). Fura2-AM was from Thermo Fisher Scientific. Rapamycin and human AngII were obtained from EMD Millipore (Burlington, MA). Unless otherwise stated, all other chemicals and reagents were purchased from Sigma (St Louis, MO, USA).

Antibodies

Polyclonal rabbit antibodies against: VAP-33 (Cat. No. A304-366A-T); VAPB (Cat. No. A302-894A-T); ORP3 (Cat. No. A304-557A-1), were all obtained from Bethyl Laboratories (Montgomery, TX, USA). The polyclonal rabbit antibody against STIM1 (Cat. No. 4916S) and the monoclonal mouse antibody against α-tubulin (Cat. No. 2144S), were from Cell Signaling Technology (Danvers, MA). The secondary fluorescent antibodies (IRDye® 680LT goat anti-rabbit and IRDye® 800CW goat anti-mouse) were both from LI-COR. All primary antibodies were used at 1:1000 and the secondary antibodies at 1:5000 dilutions.

DNA constructs

The ORP3-mCherry construct was created by cloning the amplified ORP3 cDNA sequence (NM_015550.3, purchased from Dharmacon, clone ID: 3909164) into GFP-N1 plasmid (for primers, see Table S1) using HindIII and KpnI restriction sites. The GFP sequence was then replaced with mCherry using AgeI and BsrGI sites. The resulting construct has a linker sequence AVPRARDPPVAT between ORP3 and GFP. The mCherry-VAPB construct was a gift from Christopher Stefan (UCL, London, UK) and the mCherry-Sec61B-C-18 was Addgene plasmid #55129 (deposited by Michael Davidson). To create the T2A-based vector, which contained the ORP3 and VAPB sequences in the same plasmid, the NES-Sluc-GRP1PH sequence was replaced with the PCR-amplified sequence of VAPB in our recently introduced L10-mVenus-T2A-NES-Sluc-GRP1PH construct (Tóth et al., 2019) using EcoRI and BamHI enzyme sites. In the second step, the T2A-VAPB piece was PCR-amplified, and then inserted after the mCherry sequence in the ORP3-mCherry plasmid using Bsp1407I and NotI enzymes. The FKBP-ORP3-mCherry construct was created by amplifying the FKBP sequence with PCR and inserting it into the ORP3-mCherry construct by replacing the PH domain of the protein (30–154 amino acids), using the SalI and EcoRI sites. The SalI site is present in the ORP3 sequence, whereas the EcoRI site was generated by site directed mutagenesis. Mutations (H631/632A, K829A, K837A, FF854/855IL and WY863/869LL) were introduced in the ORP3-mCherry, as well as in the ORP3-mCherry-T2A-VAPB constructs using the primers (see Table S1) using the Quik-change mutagenesis kit (Promega, Madison, WI, USA). To generate the C-terminal truncated mutants, the ORP3 sequence lacking last 35 amino acids was amplified by PCR and ligated back to the original template constructs using the NheI and AgeI restriction enzymes. In the case of the VAPB containing variants, the original ORP3 sequence was replaced with the truncated version. Venus tagged ORP3 proteins were made by replacing the mCherry sequence with the monomeric Venus (N1-mVenus, containing the A206K mutation) using AgeI and Bsp1407I enzymes. The mRFP-STIM1 construct (Várnai et al., 2007), as well as the BRET-based lipid-sensors for PIPs (Tóth et al., 2016), cholesterol and PtdSer (Sohn et al., 2018), or PA and DAG (https://www.biorxiv.org/content/10.1101/677229v1) were described earlier. The BRET-based cytoplasmic-Ca^{2+}-sensor was described in Gulyás et al. (2015) and the single-plasmid versions of the recruitable lipid-phosphatase system in Tóth et al. (2012).

Cell culture

HEK293T, COS-7 (both from ATCC) and the HEK293-AT1 cells (a line that stably expresses the type 1A rat angiotensin II receptor ($rAT1_AR$) (Hunyady et al., 2002) were maintained in Dulbecco's modified Eagle's medium (DMEM, Gibco 11995-065) supplemented with heat inactivated 10% fetal bovine serum, 50 U/ml penicillin and 50 µg/ml streptomycin (Gibco, 15140-122) together with 5 µg/ml Plasmocin (InvivoGen) as a mycoplasma prophylactic (culture media) in a 5% humidified CO_2 incubator at 37°C in tissue culture flasks (Thermo Fisher Scientific, 178905). Cell lines were regularly tested for mycoplasma contamination.

Western blot experiments

HEK293-AT1 cells were plated at a density of 3×10^5 cells/well in 6-well plates in culture medium at 37°C. One day later, the cells were transfected with 200 µl transfection mixture containing the indicated DNA constructs and 2 µl/dish Lipofectamine 2000. After 24 h, the plate was transferred on ice, and the cells were scraped into 300 µl RIPA buffer. After centrifuging the samples (15,000 ***g***, 10 min at 4°C), SDS sample buffer was added to the supernatant and samples boiled at 95°C for 5 min. Samples were loaded onto 8–16% precast SDS gels (Invitrogen, Carlsbad CA) and run for 90 min at 130 V at room temperature. The proteins were transferred to nitrocellulose membranes and incubated with the respective primary and secondary antibodies. The blots were then scanned with an Odyssey fluorescence imager (LI-COR, NE).

BRET measurements

For BRET measurements, HEK293 cells were seeded at a density of 7×10^5 cells/ml in culture medium. The transfection mixture contained 0.5 µl/well Lipofectamine 2000 and 0.2 µg/well total DNA from the indicated constructs in 50 µl/well Opti-MEM (Gibco, 31985-070). After incubation, the mixture was gently mixed with 100 µl/well cell suspension and seeded onto poly-L-lysine-treated white 96-well, flat bottom microplates (7×10^4 cells/well). Poly-L-lysine (Sigma, P8920, diluted to 0.001%) treatment was for 1 h and then removed to dryness before cell plating. BRET measurements were performed 25–26 h after transfection. Cells were washed once with a modified Krebs–Ringer buffer (50 µl) (120 mM NaCl, 4.7 mM KCl, 1.2 mM $CaCl_2$, 0.7 mM $MgSO_4$, 10 mM glucose and 10 mM Na-HEPES, pH 7.4) then incubated in the same medium for 30 min at 37°C. Coelenterazine h (the cell-permeable luciferase substrate) was dissolved in the modified Krebs–Ringer buffer (5 µM final concentration) and added in 40 µl/well volume. Measurements were then made at 37°C using a Tristar2 LB 942 Multimode Microplate Reader (Berthold Technologies). The emitted intensities were recorded using 475/20 and 540/40 nm emission filters. Detection time was 500 ms for each wavelength. The indicated reagents were added manually in 10 µl after dissolving in modified Krebs–Ringer buffer. For the stimulations, the plates were unloaded, which resulted in interruption of the recordings. To calculate changes in the PM lipid levels, BRET ratios were calculated by dividing the intensities recorded in the 540/40 nm filter by those recorded at the 475/20 wavelengths. These ratios were then normalized to the baseline and the percent changes were calculated (Tóth et al., 2019). In case of Ca^{2+} measurements, the intensities were normalized to the average values of the last three data points recorded before stimulation.

Confocal microscopy

COS-7 and HEK293-AT1 cells were seeded at a density of 3×10^4 cells/well on IBIDI 8-well µSlides and cultured at 37°C for 1 day. For transfection, the culture medium was changed to 200 µl transfection mixture containing the DNA constructs (0.2 µg total DNA/dish) and 0.33 µl/dish Lipofectamine 2000. 6 h later, the medium was changed to 300 µl supplemented DMEM medium. Cells were inspected 24–26 h after transfection using a Zeiss LSM 710 laser confocal microscope with a 63×/1.4 oil-immersion objective. Cells were kept in modified Krebs–Ringer buffer (described above) at room temperature during the experiments. Post-acquisition picture analysis was performed using Fiji and Photoshop (Adobe) software. Only linear changes were made during picture analysis and processing.

TIRF microscopy

HEK293-AT1 cells were plated on 35 mm dishes at a density of 3×10^5 cells/dish. One day later, the cells were transfected with 200 µl transfection mixture containing the indicated DNA constructs (0.6 µg each) and 2 µl/dish Lipofectamine 2000. Cells were analyzed 20–24 h after transfection using a Nikon Eclipse TiE inverted microscope equipped with a TIRF module.

Excitation was provided by a Nikon TIRF illuminator with a fiber-coupled LUN-V four-line laser launch (Nikon). Emitted intensities were acquired by a Zyla 5.5 EMCCD camera (Andor) through a Lambda 10-2 emission wheel (Sutter Instruments). mVenus and mRFP fluorescence were imaged with 488 nm and 561 nm excitation respectively, with a dual-emission filter collecting 505–550 nm and 570–620 nm (Chroma). Cells were kept in the modified Krebs–Ringer buffer at 37°C. For this, the stage and the 1.45 NA 100× plan-apochromatic oil-immersion objective (Nikon) were heated. For calculating the normalized PM intensities, images were background subtracted, then the average intensities were estimated on the entire image excluding the pixel values with 0. For normalization, each average intensity value was divided with the average value of the last three points acquired before the stimulation. Images were acquired every 10 s. The addition of stimuli was carried out manually after the fifth frame. Post-acquisition picture analysis was performed using Fiji and Photoshop (Adobe) software.

Knockdown experiments

HEK293-AT1 cells were plated on IBIDI 8-well µSlides or on 96-well microplates at a density of 10^4 cells/well. One day later, cells were transfected with 20 µl (for TIRF) or 50 µl (for BRET) transfection mixture containing the indicated siRNA (20 pmol/well) [r(GGGAAGACCUCAAUUACCA)dTdT sense sequence for Stim1; AllStars negative control siRNA, Cat. No. 1027280, both from Qiagen] and 0.75 µl/dish Lipofectamine RNAiMAX (Thermo Fisher Scientific, Cat. No. 13778150). On the next day, the medium was changed to fresh culture medium. On the fourth day, cells were transfected with the indicated DNA constructs with a mixture that contained 0.15 µg or 0.05 µg DNA and 0.75 µl or 0.5 µl Lipofectamine 2000 for TIRF and BRET experiments, respectively. For *STIM1* gene silencing, a duplex customized siRNA was used (Qiagen). Cells were analyzed 24–26 h after transfection, as detailed above for the TIRF and BRET measurements.

Statistical analysis and data plotting

For data plotting and statistical analysis, the GraphPad Prism (San Diego, CA) software was used. Specific statistical analyses are given in the figure legends for each experiment.

Acknowledgements

Confocal imaging was performed in the Microscopy Core of NICHD with the kind assistance of Drs Vincent Schram and Lynne Holtzclaw. The technical assistance of Kata Szabolcsi in the early phase of this work is highly appreciated.

Competing interests

The authors declare no competing or financial interests.

Author contributions

Conceptualization: G.G., Y.J.K., P.V., T.B.; Methodology: G.G., M.S.; Formal analysis: G.G.; Investigation: G.G.; Resources: M.S., Y.J.K.; Writing - original draft: G.G.; Writing - review & editing: T.B.; Supervision: P.V.; Project administration: T.B.; Funding acquisition: P.V., T.B.

Funding

This work was partly supported by the Intramural Research Program of the Eunice Kennedy Shriver National Institute of Child Health and Human Development of the National Institutes of Health (HD000196-20). P.V. was supported by the National Research, Development and Innovation Fund (NKFIH K105006). Deposited in PMC for release after 12 months.

Supplementary information

Supplementary information available online at
http://jcs.biologists.org/lookup/doi/10.1242/jcs.237388.supplemental

Peer review history

The peer review history is available online at https://jcs.biologists.org/lookup/doi/10.1242/jcs.237388.reviewer-comments.pdf

References

Antonny, B., Bigay, J. and Mesmin, B. (2018). The oxysterol-binding protein cycle: burning off PI(4)P to transport cholesterol. *Annu. Rev. Biochem.* **87**, 809-837. doi:10.1146/annurev-biochem-061516-044924

Baba, T., Toth, D. J., Sengupta, N., Kim, Y. J. and Balla, T. (2019). Phosphatidylinositol 4,5-bisphosphate controls Rab7 and PLEKHM1 membrane cycling during autophagosome-lysosome fusion. *EMBO J.* **38**, e100312. doi:10.15252/embj.2019102837

Beh, C. T., McMaster, C. R., Kozminski, K. G. and Menon, A. K. (2012). A detour for yeast oxysterol binding proteins. *J. Biol. Chem.* **287**, 11481-11488. doi:10.1074/jbc.R111.338400

Bojjireddy, N., Botyanszki, J., Hammond, G., Creech, D., Peterson, R., Kemp, D. C., Snead, M., Brown, R., Morrison, A., Wilson, S. et al. (2014). Pharmacological and genetic targeting of the PI4KA enzyme reveals its important role in maintaining plasma membrane phosphatidylinositol 4-phosphate and phosphatidylinositol 4,5-bisphosphate levels. *J. Biol. Chem.* **289**, 6120-6132. doi:10.1074/jbc.M113.531426

Broad, L. M., Braun, F.-J., Lievremont, J.-P., Bird, G. S. J., Kurosaki, T. and Putney, J. W.Jr. (2001). Role of the phospholipase C-inositol 1,4,5-trisphosphate pathway in calcium release-activated calcium current and capacitative calcium entry. *J. Biol. Chem.* **276**, 15945-15952. doi:10.1074/jbc.M011571200

Chung, J., Torta, F., Masai, K., Lucast, L., Czapla, H., Tanner, L. B., Narayanaswamy, P., Wenk, M. R., Nakatsu, F. and De Camilli, P. (2015). Intracellular transport. PI4P/phosphatidylserine countertransport at ORP5- and ORP8-mediated ER-plasma membrane contacts. *Science* **349**, 428-432. doi:10.1126/science.aab1370

Csordás, G., Renken, C., Várnai, P., Walter, L., Weaver, D., Buttle, K. F., Balla, T., Mannella, C. A. and Hajnoczky, G. (2006). Structural and functional features and significance of the physical linkage between ER and mitochondria. *J. Cell Biol.* **174**, 915-921. doi:10.1083/jcb.200604016

Darbyson, A. and Ngsee, J. K. (2016). Oxysterol-binding protein ORP3 rescues the Amyotrophic Lateral Sclerosis-linked mutant VAPB phenotype. *Exp. Cell Res.* **341**, 18-31. doi:10.1016/j.yexcr.2016.01.013

de Saint-Jean, M., Delfosse, V., Douguet, D., Chicanne, G., Payrastre, B., Bourguet, W., Antonny, B. and Drin, G. (2011). Osh4p exchanges sterols for phosphatidylinositol 4-phosphate between lipid bilayers. *J. Cell Biol.* **195**, 965-978. doi:10.1083/jcb.201104062

Del Bel, L. M. and Brill, J. A. (2018). Sac1, a lipid phosphatase at the interface of vesicular and nonvesicular transport. *Traffic* **19**, 301-318. doi:10.1111/tra.12554

Deng, X., Wang, Y., Zhou, Y., Soboloff, J. and Gill, D. L. (2009). STIM and Orai: dynamic intermembrane coupling to control cellular calcium signals. *J. Biol. Chem.* **284**, 22501-22505. doi:10.1074/jbc.R109.018655

Dong, J., Du, X., Wang, H., Wang, J., Lu, C., Chen, X., Zhu, Z., Luo, Z., Yu, L., Brown, A. J. et al. (2019). Allosteric enhancement of ORP1-mediated cholesterol transport by PI(4,5)P2/PI(3,4)P2. *Nat. Commun.* **10**, 829. doi:10.1038/s41467-019-08791-0

Gatta, A. T. and Levine, T. P. (2017). Piecing Together the Patchwork of Contact Sites. *Trends Cell Biol.* **27**, 214-229. doi:10.1016/j.tcb.2016.08.010

Ghai, R., Du, X., Wang, H., Dong, J., Ferguson, C., Brown, A. J., Parton, R. G., Wu, J.-W. and Yang, H. (2017). ORP5 and ORP8 bind phosphatidylinositol-4, 5-biphosphate (PtdIns(4,5)P 2) and regulate its level at the plasma membrane. *Nat. Commun.* **8**, 757. doi:10.1038/s41467-017-00861-5

Giordano, F., Saheki, Y., Idevall-Hagren, O., Colombo, S. F., Pirruccello, M., Milosevic, I., Gracheva, E. O., Bagriantsev, S. N., Borgese, N. and De Camilli, P. (2013). PI(4,5)P(2)-dependent and Ca(2+)-regulated ER-PM interactions mediated by the extended synaptotagmins. *Cell* **153**, 1494-1509. doi:10.1016/j.cell.2013.05.026

Gulyás, G., Tóth, J. T., Tóth, D. J., Kurucz, I., Hunyady, L., Balla, T. and Várnai, P. (2015). Measurement of inositol 1,4,5-trisphosphate in living cells using an improved set of resonance energy transfer-based biosensors. *PLoS ONE* **10**, e0125601. doi:10.1371/journal.pone.0125601

Gulyás, G., Radvánszki, G., Matuska, R., Balla, A., Hunyady, L., Balla, T. and Várnai, P. (2017). Plasma membrane phosphatidylinositol 4-phosphate and 4,5-bisphosphate determine the distribution and function of K-Ras4B but not H-Ras proteins. *J. Biol. Chem.* **292**, 18862-18877. doi:10.1074/jbc.M117.806679

Hammond, G. R. V., Fischer, M. J., Anderson, K. E., Holdich, J., Koteci, A., Balla, T. and Irvine, R. F. (2012). PI4P and PI(4,5)P2 are essential but independent lipid determinants of membrane identity. *Science* **337**, 727-730. doi:10.1126/science.1222483

Hunyady, L., Baukal, A. J., Gáborik, Z., Olivares-Reyes, J. A., Bor, M., Szaszák, M., Lodge, R., Catt, K. J. and Balla, T. (2002). Differential PI 3-kinase dependence of early and late phases of recycling of the internalized AT1 angiotensin receptor. *J. Cell Biol.* **157**, 1211-1222. doi:10.1083/jcb.200111013

Kentala, H., Weber-Boyvat, M. and Olkkonen, V. M. (2016). OSBP-related protein family: mediators of lipid transport and signaling at membrane contact sites. *Int. Rev. Cell Mol. Biol.* **321**, 299-340. doi:10.1016/bs.ircmb.2015.09.006

Kim, Y. J., Guzman-Hernandez, M.-L., Wisniewski, E. and Balla, T. (2015). Phosphatidylinositol-phosphatidic acid exchange by Nir2 at ER-PM contact sites maintains phosphoinositide signaling competence. *Dev. Cell* **33**, 549-561. doi:10.1016/j.devcel.2015.04.028

Korzeniowski, M. K., Popovic, M. A., Szentpetery, Z., Varnai, P., Stojilkovic, S. S. and Balla, T. (2009). Dependence of STIM1/Orai1-mediated calcium entry on plasma membrane phosphoinositides. *J. Biol. Chem.* **284**, 21027-21035. doi:10.1074/jbc.M109.012252

Lehto, M., Mayranpaa, M. I., Pellinen, T., Ihalmo, P., Lehtonen, S., Kovanen, P. T., Groop, P.-H., Ivaska, J. and Olkkonen, V. M. (2008). The R-Ras interaction partner ORP3 regulates cell adhesion. *J. Cell Sci.* **121**, 695-705. doi:10.1242/jcs.016964

Liou, J., Kim, M. L., Heo, W. D., Jones, J. T., Myers, J. W., Ferrell, J. E., Jr and Meyer, T. (2005). STIM is a Ca2+ sensor essential for Ca2+-store-depletion-triggered Ca2+ influx. *Curr. Biol.* **15**, 1235-1241. doi:10.1016/j.cub.2005.05.055

Liou, J., Fivaz, M., Inoue, T. and Meyer, T. (2007). Live-cell imaging reveals sequential oligomerization and local plasma membrane targeting of stromal interaction molecule 1 after Ca2+ store depletion. *Proc. Natl. Acad. Sci. USA* **104**, 9301-9306. doi:10.1073/pnas.0702866104

Loewen, C. J. R., Roy, A. and Levine, T. P. (2003). A conserved ER targeting motif in three families of lipid binding proteins and in Opi1p binds VAP. *EMBO J.* **22**, 2025-2035. doi:10.1093/emboj/cdg201

Maeda, K., Anand, K., Chiapparino, A., Kumar, A., Poletto, M., Kaksonen, M. and Gavin, A.-C. (2013). Interactome map uncovers phosphatidylserine transport by oxysterol-binding proteins. *Nature* **501**, 257-261. doi:10.1038/nature12430

Manford, A. G., Stefan, C. J., Yuan, H. L., Macgurn, J. A. and Emr, S. D. (2012). ER-to-plasma membrane tethering proteins regulate cell signaling and ER morphology. *Dev. Cell* **23**, 1129-1140. doi:10.1016/j.devcel.2012.11.004

Mesmin, B., Bigay, J., Moser von Filseck, J., Lacas-Gervais, S., Drin, G. and Antonny, B. (2013). A four-step cycle driven by PI(4)P hydrolysis directs sterol/PI(4)P exchange by the ER-Golgi tether OSBP. *Cell* **155**, 830-843. doi:10.1016/j.cell.2013.09.056

Mochizuki, S., Miki, H., Zhou, R., Kido, Y., Nishimura, W., Kikuchi, M. and Noda, Y. (2018). Oxysterol-binding protein-related protein (ORP) 6 localizes to the ER and ER-plasma membrane contact sites and is involved in the turnover of PI4P in cerebellar granule neurons. *Exp. Cell Res.* **370**, 601-612. doi:10.1016/j.yexcr.2018.07.025

Nakatsu, F., Baskin, J. M., Chung, J., Tanner, L. B., Shui, G., Lee, S. Y., Pirruccello, M., Haio, M., Ingolia, N. T., Wenk, M. R. et al. (2012). PtdIns4P synthesis by PI4KIIIa at the plasma membrane and its impact on plasma membrane identity. *J. Cell Biol.* **199**, 1003-1016. doi:10.1083/jcb.201206095

Njeru, S. N., Kraus, J., Meena, J. K., Lechel, A., Katz, S.-F., Kumar, M., Knippschild, U., Azoitei, A., Wezel, F., Bolenz, C. et al. (2019). Aneuploidy-inducing gene knockdowns overlap with cancer mutations and identify Orp3 as a B-cell lymphoma suppressor. *Oncogene* **39**, 1445-1465. doi:10.1038/s41388-019-1073-2

Pietrangelo, A. and Ridgway, N. D. (2018). Bridging the molecular and biological functions of the oxysterol-binding protein family. *Cell. Mol. Life Sci.* **75**, 3079-3098. doi:10.1007/s00018-018-2795-y

Pulli, I., Lassila, T., Pan, G., Yan, D., Olkkonen, V. M. and Törnquist, K. (2018). Oxysterol-binding protein related-proteins (ORPs) 5 and 8 regulate calcium signaling at specific cell compartments. *Cell Calcium* **72**, 62-69. doi:10.1016/j.ceca.2018.03.001

Santos, M. F., Rappa, G., Karbanová, J., Kurth, T., Corbeil, D. and Lorico, A. (2018). VAMP-associated protein-A and oxysterol-binding protein-related protein 3 promote the entry of late endosomes into the nucleoplasmic reticulum. *J. Biol. Chem.* **293**, 13834-13848. doi:10.1074/jbc.RA118.003725

Sohn, M., Korzeniowski, M., Zewe, J. P., Wills, R. C., Hammond, G. R. V., Humpolickova, J., Vrzal, L., Chalupska, D., Veverka, V., Fairn, G. D. et al. (2018). PI(4,5)P2 controls plasma membrane PI4P and PS levels via ORP5/8 recruitment to ER-PM contact sites. *J. Cell Biol.* **217**, 1797-1813. doi:10.1083/jcb.201710095

Stefan, C. J., Manford, A. G., Baird, D., Yamada-Hanff, J., Mao, Y. and Emr, S. D. (2011). Osh proteins regulate phosphoinositide metabolism at ER-plasma membrane contact sites. *Cell* **144**, 389-401. doi:10.1016/j.cell.2010.12.034

Szabadkai, G., Bianchi, K., Várnai, P., De Stefani, D., Wieckowski, M. R., Cavagna, D., Nagy, A. I., Balla, T. and Rizzuto, R. (2006). Chaperone-mediated coupling of endoplasmic reticulum and mitochondrial Ca2+ channels. *J. Cell Biol.* **175**, 901-911. doi:10.1083/jcb.200608073

Tong, J., Yang, H., Yang, H., Eom, S. H. and Im, Y. J. (2013). Structure of Osh3 reveals a conserved mode of phosphoinositide binding in oxysterol-binding proteins. *Structure* **21**, 1203-1213. doi:10.1016/j.str.2013.05.007

Tong, J., Manik, M. K., Yang, H. and Im, Y. J. (2016). Structural insights into nonvesicular lipid transport by the oxysterol binding protein homologue family. *Biochim. Biophys. Acta* **1861**, 928-939. doi:10.1016/j.bbalip.2016.01.008

Tóth, D. J., Tóth, J., Gulyás, G., Balla, A., Balla, T., Hunyady, L. and Várnai, P. (2012). Acute depletion of plasma membrane Phosphatidylinositol 4,5-bisphosphate impairs specific steps in G protein-coupled receptor endocytosis. *J. Cell Sci.* **125**, 3013. doi:10.1242/jcs.115048

Tóth, J. T., Gulyás, G., Tóth, D. J., Balla, A., Hammond, G. R. V., Hunyady, L., Balla, T. and Várnai, P. (2016). BRET-monitoring of the dynamic changes of inositol lipid pools in living cells reveals a PKC-dependent PtdIns4P increase upon EGF and M3 receptor activation. *Biochim. Biophys. Acta* **1861**, 177-187. doi:10.1016/j.bbalip.2015.12.005

Tóth, J. T., Gulyás, G., Hunyady, L. and Várnai, P. (2019). Development of nonspecific BRET-based biosensors to monitor plasma membrane inositol lipids in living cells. *Methods Mol. Biol.* **1949**, 23-34. doi:10.1007/978-1-4939-9136-5_3

Várnai, P., Tóth, B., Tóth, D. J., Hunyady, L. and Balla, T. (2007). Visualization and manipulation of plasma membrane-endoplasmic reticulum contact sites indicates the presence of additional molecular components within the STIM1-Orai1 Complex. *J. Biol. Chem.* **282**, 29678-29690. doi:10.1074/jbc.M704339200

Várnai, P., Gulyás, G., Tóth, D. J., Sohn, M., Sengupta, N. and Balla, T. (2017). Quantifying lipid changes in various membrane compartments using lipid binding protein domains. *Cell Calcium* **64**, 72-82. doi:10.1016/j.ceca.2016.12.008

Wang, H., Ma, Q., Qi, Y., Dong, J., Du, X., Rae, J., Wang, J., Wu, W.-F., Brown, A. J., Parton, R. G. et al. (2018). ORP2 delivers cholesterol to the plasma membrane in exchange for phosphatidylinositol 4, 5-bisphosphate (PI(4,5)P2). *Mol. Cell* **73**, 458-473.e7. doi:10.1016/j.molcel.2018.11.014

Weber-Boyvat, M., Kentala, H., Lilja, J., Vihervaara, T., Hanninen, R., Zhou, Y., Peränen, J., Nyman, T. A., Ivaska, J. and Olkkonen, V. M. (2015). OSBP-related protein 3 (ORP3) coupling with VAMP-associated protein A regulates R-Ras activity. *Exp. Cell Res.* **331**, 278-291. doi:10.1016/j.yexcr.2014.10.019

Wong, L. H., Gatta, A. T. and Levine, T. P. (2018). Lipid transfer proteins: the lipid commute via shuttles, bridges and tubes. *Nat. Rev. Mol. Cell Biol.* **20**, 85-101. doi:10.1038/s41580-018-0071-5

Wu, H., Carvalho, P. and Voeltz, G. K. (2018). Here, there, and everywhere: the importance of ER membrane contact sites. *Science* **361**. doi:10.1126/science.aan5835

Zewe, J. P., Wills, R. C., Sangappa, S., Goulden, B. D. and Hammond, G. R. V. (2018). SAC1 degrades its lipid substrate PtdIns4P in the endoplasmic reticulum to maintain a steep chemical gradient with donor membranes. *eLife* **7**, e35588. doi:10.7554/eLife.35588

Zhang, S. L., Yu, Y., Roos, J., Kozak, J. A., Deerinck, T. J., Ellisman, M. H., Stauderman, K. A. and Cahalan, M. D. (2005). STIM1 is a Ca2+ sensor that activates CRAC channels and migrates from the Ca2+ store to the plasma membrane. *Nature* **437**, 902-905. doi:10.1038/nature04147